UNIVERSITY OF
Southampton
Institute of Sound and
Vibration Research

ISVR Technical Memorandum

Fluid Coupling between the Elements in a Discrete Model of Cochlear Mechanics

S.J. Elliott, B. Lineton and G. Ni

ISVR Technical Memorandum No 990

October 2010

SCIENTIFIC PUBLICATIONS BY THE ISVR

Technical Reports are published to promote timely dissemination of research results by ISVR personnel. This medium permits more detailed presentation than is usually acceptable for scientific journals. Responsibility for both the content and any opinions expressed rests entirely with the author(s).

Technical Memoranda are produced to enable the early or preliminary release of information by ISVR personnel where such release is deemed to the appropriate. Information contained in these memoranda may be incomplete, or form part of a continuing programme; this should be borne in mind when using or quoting from these documents.

Contract Reports are produced to record the results of scientific work carried out for sponsors, under contract. The ISVR treats these reports as confidential to sponsors and does not make them available for general circulation. Individual sponsors may, however, authorize subsequent release of the material.

UNIVERSITY OF SOUTHAMPTON

INSTITUTE OF SOUND AND VIBRATION RESEARCH

SIGNAL PROCESSING AND CONTROL GROUP

Fluid Coupling between the Elements in a Discrete Model of Cochlear Mechanics

by

S.J. Elliott, B. Lineton and G. Ni

ISVR Memorandum No. 990

October 2010

Modified in May 2011

Authorised for issue by

Professor R. Allen

Group Chairman

Acknowledgements

The data points for the areas of the two chambers shown in Fig. 4.1 were extracted from Fig. 2 in Zakis and Witte (2001) by Rami Saba. Jackie Young performed the simulations for Fig. 7.2.

CONTENTS

Page

List of Figures

Page

List of Tables

Page

Abstract

When analysing the coupled mechanics of the cochlea, due to the interaction between fluid coupling and basilar membrane motion, it is convenient to divide the cochlea longitudinally into a discrete number of sections. This report considers the fluid coupling in such a discrete model. The fluid coupling is analysed using a wavenumber formulation and is separated into long wavelength and short wavelength components. The short wavelength components are then seen as one of a number of sources of additional longitudinal coupling that could be incorporated into a modified model of basilar membrane dynamics. The effects of non-uniformity and asymmetry in the fluid chamber areas can then be taken into account to predict both the pressure difference between the chambers and the mean pressure. The results from the analytic formulation, in which the fluid is assumed to be incompressible, are also compared with those of an acoustic finite element model for the fluid coupling. Although the agreement is good at low frequencies, a resonance is observed at about 11 kHz due to the compressibility of the fluid, although this does not appear to affect the coupled cochlear response.

1. Introduction

The modelling of a three-dimensional cochlea can be reduced to a single dimension by the definition of a radially-averaged basilar membrane, BM, velocity and a radially-averaged pressure difference acting upon it. For numerical computations it is then convenient to divide the longitudinal variation of these parameters into a number of discrete elements, which may be taken to be an accurate representation of the continuous system if there are at least six elements within the shortest wavelength present; a condition commonly used in finite element analysis (Fahy and Gardonio, 2007).

The coupled behaviour of the cochlear dynamics, which are assumed to be linear, can then be represented by matrix representations of two separate phenomena. First, the way that the pressure distribution is determined by the fluid coupling within the cochlear chambers when driven by the BM velocity, and second, the way in which the BM dynamics respond to the imposed pressure distribution.

This kind of discrete model was used, for example, by Neely and Kim (1986), to simulate an early model of the active cochlea, and has been used by many authors since then. These discrete models have generally been applied to uniform and symmetric box models of the cochlea, using the finite difference method to represent only the long wavelength component of the fluid coupling. In this section a general approach is taken to the derivation of the discrete model, using modal BM velocity and modal pressure difference, which allows the definition of generic matrices describing the fluid coupling and BM dynamics.

A widely used geometry for the three-dimensional cochlea is the rectangular box model, as discussed by de Boer (1996), for example, and illustrated in Fig. 1.1(a). The cochlea is assumed to be uncoiled and, for the time being, to be of uniform cross section and to have symmetric fluid chambers. The lower fluid chamber is the *scala tympani*, ST, and the upper fluid chamber represents both the *scala media*, SM, and the *scala vistibuli*, SV. It is assumed that Reissner's membrane is flexible enough to play no significant part in the dynamics of the fluid motion in the upper chamber. The cochlea is driven by the motion of the stapes at the oval window. At very low frequencies the cochlear fluids can flow along the upper chamber, through the gap in

the basilar membrane at the helicotrema, and back through the lower chamber to drive the motion of the flexible round window. At audio frequencies a "slow" wave is generated by the interaction between the fluid's inertia and BM stiffness, which propagates to a frequency-dependent characteristic place, beyond which it rapidly decays. In this report, the fluid coupling in a discrete model of the cochlea is considered by investigating the pressure distribution generated by the motion of the oval window and the elements of the BM.

(a)

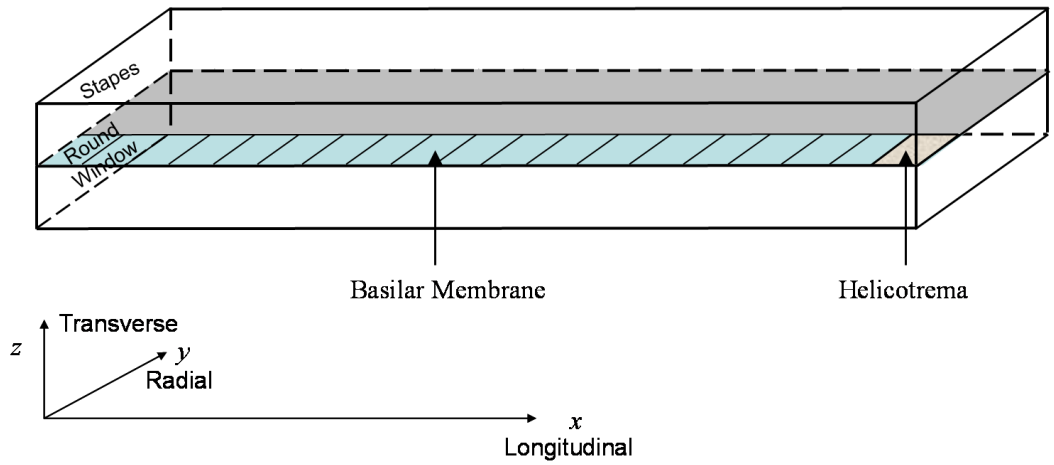

(b)

$$u_s \longrightarrow \boxed{\begin{array}{cccccccc} \frac{p(1)}{v(1)} & \frac{p(2)}{v(2)} & \cdots & \cdots & \cdots & \cdots & \frac{p(N-1)}{v(N-1)} & \frac{p(N)}{v(N)} \end{array}}$$

Fig. 1.1 *The physical box model assumed to calculate the fluid coupling (a) together with the definition of the coordinate system and (b) the discrete approximation.*

The radial variation of BM velocity over the width of the cochlear partition, *W*, is assumed to be proportional to a single modal shape, $\psi(y)$, which is independent of the distribution of the pressure acting upon it. The analysis can be generalised to the case in which the radial BM velocity is the sum of a number of such modes (Neely, 1985) but in practice the fluid coupling is relatively insensitive to the exact form of the radial BM velocity distribution and so it is reasonable to assume a single shape for this. Its upward *modal* amplitude at longitudinal position *x* is defined to be

$$v(x) = \frac{1}{W}\int_0^W \psi(y) v(x,y)\,dy, \tag{1.1}$$

where $v(x, y)$ is the longitudinal and radial distribution of complex BM velocity, at a single frequency, the dependence on which is suppressed for notational convenience. Corresponding modal pressures (Steele and Taber, 1979) in the upper and lower chambers can also be defined as

$$p_1(x) = \frac{1}{W}\int_0^W \psi(y)\, p_1(x,y,0)\,dy\,, \tag{1.2}$$

$$p_2(x) = \frac{1}{W}\int_0^W \psi(y)\, p_2(x,y,0)\,dy\,, \tag{1.3}$$

where $p_1(x, y, z)$ is the 3-D distribution of complex pressure in the upper fluid chamber and $p_2(x, y, z)$ is that in the lower fluid chamber, and the coordinate system is shown in Fig. 1.1(a).

In understanding the form of the complex pressure in the two fluid chambers, $p_1(x)$ and $p_2(x)$, it is helpful to define two alternative pressure variables (Peterson and Bogert, 1950), which are the pressure difference across the BM, $p(x)$, and the common-mode pressure $p_{\mathrm{M}}(x)$, such that

$$p(x) = p_1(x) - p_2(x), \quad p_{\mathrm{M}}(x) = \frac{p_1(x) + p_2(x)}{2}\,. \tag{1.4, 1.5}$$

The two individual fluid pressures can be written in terms of these new variables as

$$p_1(x) = p_{\mathrm{M}}(x) + p(x)/2, \quad p_2(x) = p_{\mathrm{M}}(x) - p(x)/2\,. \tag{1.6, 1.7}$$

The boundary conditions that must be obeyed by the pressure difference and common mode pressures allow a simpler analysis of these two components than the individual pressures, as noted by Lighthill (1981), who descriptively termed $p_{\mathrm{M}}(x)$ and $p(x)$ the even and odd parts of the pressure, and by de Boer (1996), who calls them the symmetric and anti-symmetric pressures.

The boundary conditions for these two components are determined by their symmetric and anti-symmetric forms. For the mean pressure, $p_1(x)$ must equal $p_2(x)$ and so the volume excitations at the oval and round windows must be equal, i.e., both inwards, and the motion of the BM must be zero. For the pressure difference, $p_1(x)$ must equal $-p_2(x)$ and so the volume excitation at the round window must be equal and opposite to that at the oval window. Transverse BM motion is also allowed in this case since the resulting excitation of the upper chamber is equal and opposite to that of the lower chamber. It is thus only the pressure difference that interacts with the BM dynamics and generates the "slow" wave motion noted above. The chambers are connected at the helicotrema, which is, for now, assumed to equalise the pressures in the two chambers, so that the pressure difference must then be zero.

If the single longitudinal variables, for modal pressure difference and modal velocity, are spatially sampled as finely as required, dividing the cochlea into *N* segments, we can define, at a single frequency, the vectors of complex pressures and velocities, **p** and **v**, to be

$$\mathbf{p} = \left[p(1), p(2), \cdots p(N) \right]^{\mathrm{T}}, \qquad \mathbf{v} = \left[v(1), v(2), \cdots v(N) \right]^{\mathrm{T}}, \qquad (1.8,1.9)$$

whose elements are shown in Fig. 1.1(b).

The BM, however, is assumed only to extend from element 2 to element $N-1$. Element 1 is used to account for the effect of the stapes velocity, shown as u_s in Fig. 1.1(b). The final element, *N*, is used to account for the behaviour of the helicotrema. With the stapes velocity set to zero, the vector of pressures due to the vector of BM velocities can be written as

$$\mathbf{p} = \mathbf{Z}_{\mathrm{FC}} \mathbf{v}, \qquad (1.10)$$

where $\mathbf{Z}_{\mathrm{FC}}$ is a matrix of impedances due to the fluid coupling. Similarly, the vector of BM velocities can be written as

$$\mathbf{v} = -\mathbf{Y}_{\mathrm{BM}} \mathbf{p}, \qquad (1.11)$$

Where $\mathbf{Y}_{\mathrm{BM}}$ is a matrix of BM admittances. The first and last diagonal elements are zero, since the BM only extends from element 2 to element $N-1$. If the BM reacts only locally, then $\mathbf{Y}_{\mathrm{BM}}$ is a diagonal matrix. In general, however, we do not need to place such restrictions on this matrix, as discussed in Section 7.

We now define the vector of pressures due to the stapes velocity, u_{s}, and with a rigid BM to be $\mathbf{z}_{\mathrm{s}}u_{\mathrm{s}}$, where $\mathbf{z}_{\mathrm{s}}$ is the vector of fluid coupling impedances from the stapes to each element along the cochlea. The total pressure vector due to both stapes motion and motion of the BM can then be written, using linear superposition, as

$$\mathbf{p} = \mathbf{z}_{\mathrm{s}}u_{\mathrm{s}} + \mathbf{Z}_{\mathrm{FC}}\mathbf{v}. \tag{1.12}$$

Since the contribution to the pressure from the stapes motion is accounted for by the first term in equation (1.12), the first column of the $\mathbf{Z}_{\mathrm{FC}}$ matrix is zero. Equations (1.11) and (1.12) can be combined to give

$$\mathbf{p} = \mathbf{z}_{\mathrm{s}}u_{\mathrm{s}} - \mathbf{Z}_{\mathrm{FC}}\mathbf{Y}_{\mathrm{BM}}\mathbf{p}, \tag{1.13}$$

so that the vector of coupled pressure differences is given by

$$\mathbf{p} = \left[\mathbf{I} + \mathbf{Z}_{\mathrm{FC}}\mathbf{Y}_{\mathrm{BM}}\right]^{-1}\mathbf{z}_{\mathrm{s}}u_{\mathrm{s}}, \tag{1.14}$$

and the vector of coupled BM velocities by

$$\mathbf{v} = -\mathbf{Y}_{\mathrm{BM}}\left[\mathbf{I} + \mathbf{Z}_{\mathrm{FC}}\mathbf{Y}_{\mathrm{BM}}\right]^{-1}\mathbf{z}_{\mathrm{s}}u_{\mathrm{s}}. \tag{1.15}$$

Fluid coupling in the box model is often described using a wavenumber analysis (Steele and Taber, 1979; de Boer, 1984). This is reproduced in the Appendix for completeness and is used in Section 2 to obtain the columns of the matrix $\mathbf{Z}_{\mathrm{FC}}$ above, required to reproduce both long wavelength and short wavelength fluid coupling. Although a rectangular cross section for the fluid chambers is assumed here, de Boer (1991) has shown that similar results are obtained if the cross section is assumed to be semi-circular.

Section 3 then illustrates the effects of these different types of fluid coupling on the predicted distributions of BM velocity along the cochlea.

The effect of fluid coupling in a non-uniform cochlea is discussed in Section 4. The discrete analysis method is then used to investigate the change in the passive response at the apical end of the cochlea when a short cochlear implant is inserted into the base.

Section 5 compares the fluid coupling results from the analytic formulation with that of a finite element model.

In Section 6 a modified form of the state space description of the cochlear mechanics is described, which includes acoustic modes in the fluid.

Finally, in Section 7, the incorporation of short wavelength fluid coupling into the BM dynamics is discussed and is shown to allow a formulation which is numerically efficient.

2. Fluid coupling in a discrete model of the uniform cochlea

In the Appendix, the conventional wavenumber analysis of fluid coupling in a uniform cochlea is briefly reviewed, following the approach of Steele and Taber (1979). The modal pressure difference in the wavenumber domain can be written as

$$P(k) = Z_{\mathrm{FC}}(k)V(k), \tag{2.1}$$

where $V(k)$ is the wavenumber spectrum of the modal BM velocity distribution along the cochlea and $Z_{\mathrm{FC}}(k)$ is the wavenumber representation of the fluid coupling impedance. It is convenient, de Boer (1984), to express $Z_{\mathrm{FC}}(k)$ in the form

$$Z_{\mathrm{FC}}(k) = i2\omega\rho Q(k), \tag{2.2}$$

where $Q(k)$ has the dimensions of length and has been termed the "equivalent height" (La Rochefoucauld and Olson, 2007). The factor of 2 is introduced here, compared with de Boer (1984), since the pressure difference is being used here rather than the pressure semi difference. Fig. 2.1 shows the variation of $Q(k)/H$ with kH, where H is the physical height of one fluid chamber, calculated from the equations derived in the Appendix, for the parameters listed in Table 2.1. The BM is assumed to be located on one side of the cochlear partition and its width, *B*, is assumed to be 0.3 times that of the cochlear partition, *W*, in this example. The change in the fluid coupling when the ratio of *B* to *W* varies is discussed in the Appendix.

The fluid coupling impedance may be decomposed into two components, one due to the long wavelength fluid coupling, $Z_{\mathrm{L}}(k)$ and one due to the short wavelength fluid coupling, $Z_{\mathrm{S}}(k)$, so that

$$Z_{\mathrm{FC}}(k) = Z_{\mathrm{L}}(k) + Z_{\mathrm{S}}(k). \tag{2.3}$$

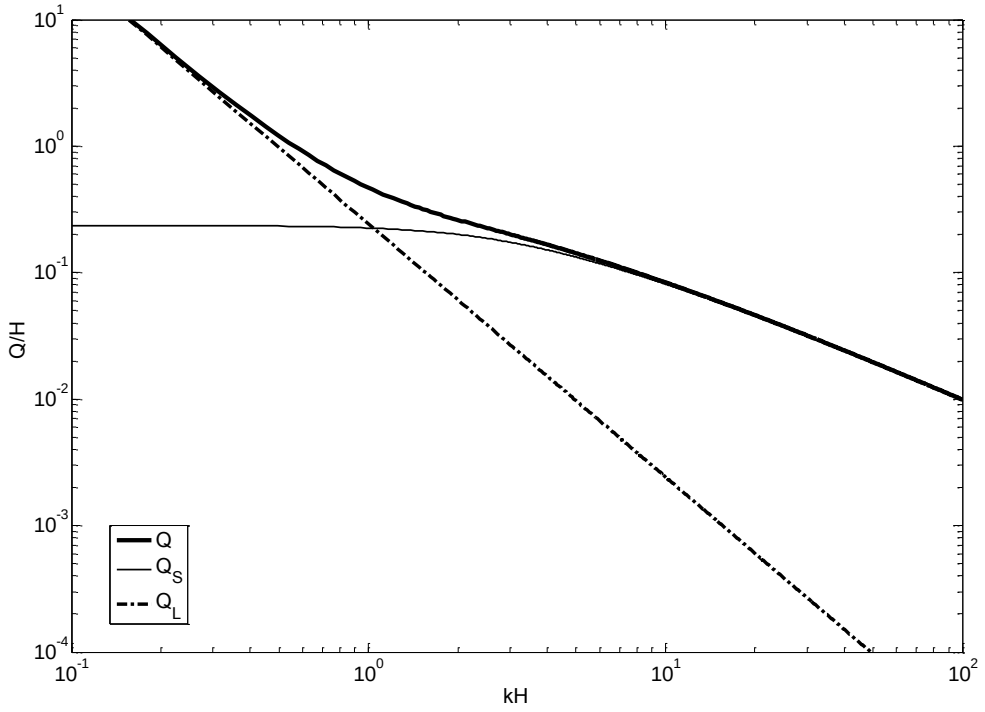

Fig. 2.1 *The wavenumber description of the total fluid coupling in the box model of the cochlea (thick solid line) and its decomposition into long wavelength components (dot-dashed) and short wavelength components (faint solid line).*

It should be noted that the short wavelength term here is different from the "short wave" component discussed by de Boer (1996), for example, where the limit for large k is taken to yield a fluid coupling impedance proportional to $1/k$. The definition of $Z_{\mathrm{S}}(k)$ used here includes *all* the elements of $Z_{\mathrm{FC}}(k)$ except the term $Z_{\mathrm{L}}(k)$. This definition is, however, similar to that used by Nobili and Mammano (1993) for the long-range and short-range parts of their fluid coupling Green's function. This is because the long wavelength components are associated with the pressure response some distance from the source of excitation on the BM, and so could also be descriptively called the far field components, whereas the short wavelength components are, as we will see, associated with the pressure response close to the source of excitation and so could also be called the near field components. Note, however, that formally speaking both terms describe the behaviour in the hydrodynamic near field of the source, if the fluid is sufficiently incompressible that the wavelength is large compared with the length of the cochlea, so that it is the geometric near and far fields we are referring to here.

Table 2.1 *Values of physical parameters used for the simulations in Sections 2 and 3.*

Variable	Parameter	Value
L	Length of cochlea	35 mm
W	Width of fluid chamber	1 mm
B	Width of basilar membrane	0.3 mm
H	Physical height of single fluid chamber	1 mm
h	Effective chamber height for 1D model	4.1 mm
ρ	Density of fluid	1,000 kg.m^{-3}
N	Number of elements in discrete model	512
$\Delta = L/N$	Length of element	68 μm
m_0	BM mass, 1D model	0.29 kg.m^{-2}
m_{3D}	BM mass, 3D model	0.05 kg.m^{-2}
ω_0	BM natural frequency distribution	$\omega_B\, e^{-x/l}$
ω_B	BM natural frequency at base	$2\pi \times 20{,}000$ rad.s^{-1}
l	Natural frequency length scale	7 mm
$s_0(x)$	BM stiffness	$m_0\ \omega_0^2(x)$
ζ_0	BM damping ratio	0.2
r_0	BM damping	$2m_0\zeta_0\omega_0$
d	Characteristic distance	0.8 mm

The long wavelength fluid component is defined so that it obeys the equation derived from a one dimensional analysis of the incompressible fluid coupling, derived as a limiting case of the general formulation in the appendix, equation (A29), and given by

$$\frac{\partial^2 p_L(x)}{\partial x^2} = -\frac{2i\omega\rho}{h} v(x), \tag{2.4}$$

where h is the effective chamber height, assumed here to be independent of x, so that in the wavenumber domain

$$P_{\mathrm{L}}(k) = \frac{2i\omega\rho}{k^2 h} V(k), \quad Z_{\mathrm{L}}(k) = \frac{2i\omega\rho}{k^2 h} \quad \text{and} \quad Q_{\mathrm{L}}(k) = \frac{1}{k^2 h}. \qquad (2.5, 2.6, 2.7)$$

We can thus decompose $Q(k)$ in equation (2.2) as in equation (2.3) and define the short wavelength component to be

$$Q_{\mathrm{S}}(k) = Q(k) - Q_{\mathrm{L}}(k). \qquad (2.8)$$

It is shown in the Appendix that the effective height can be expressed in terms of the physical height of the fluid chamber, H, its width, W, and the width of the basilar membrane, B, as

$$h = \frac{\pi^2 WH}{8B}, \qquad (2.9)$$

so that for the ratio of B to W used here, 0.3, the effective chamber height is about 4.1 times the physical chamber height.

Fig. 2.1 shows the two components of $Q(k)$ corresponding to the long wavelength and short wavelength components. For long wavelengths, small k, the short wavelength coupling, $Q_{\mathrm{S}}(k)$, becomes a constant, which can be interpreted as an effective added BM thickness, T, whose value as a function of B/W is discussed in the Appendix. For short wavelengths, large k, $Q_{\mathrm{S}}(k)$ is equal to $1/k$, whatever the BM width.

To illustrate the change in the pressure distribution with wavenumber, Fig. 2.2 shows the equipressure contours in a cross section of the box model for various values of kH.

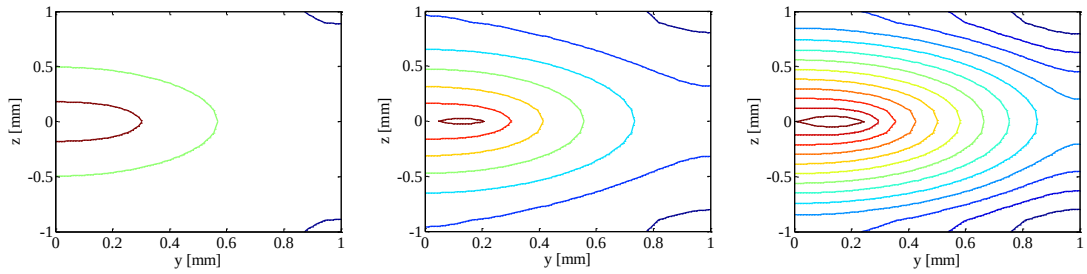

Fig. 2.2 *Contours of equal pressure, at 5 dB intervals, in a cross section of the box model of the cochlea when the BM, which is on the left hand third of the cochlear partition in this case, has a longitudinally sinusoidal variation with normalised wavenumbers of kH = 1.5 (left), kH = 3 (centre) and kH = 6 (right), corresponding to wavelengths* $\lambda \approx 4H$, $\lambda \approx 2H$ *and* $\lambda \approx H$, *where H is the physical height of a single chamber.*

For low values of *kH* the wavelength of the longitudinal BM vibration is much greater than the height of the fluid chamber, and so $Q_{\mathrm{S}}(k)$ is very small compared with $Q_{\mathrm{L}}(k)$, which is proportional to $1/k^2$, and the pressure is almost uniform across the cross sectional area. As the wavelength becomes comparable with the height, $Q_{\mathrm{S}}(k)$ becomes comparable with $Q_{\mathrm{L}}(k)$ and significant variation is seen in the pressure across the cross section. When the wavelength is small compared with the height, $Q_{\mathrm{S}}(k)$ becomes equal to $1/k$, which is large compared with $Q_{\mathrm{L}}(k)$ and the pressure is much greater close to the BM than it is in the rest of the fluid chamber. The short wavelength component of the fluid coupling can thus be thought of as being due to the near field of the BM source, as opposed to the long wavelength component, which can be thought of as being due to the far field.

The long wavelength component is often referred to as 1D fluid coupling, since it can be readily derived from a one-dimensional box model of the cochlea with the assumption that the wavelength is long compared with the height of the fluid chamber (de Boer 1996). The full fluid coupling model, including short wavelength components, is then referred to as 3D fluid coupling. It must be emphasised, however, that when the cochlear mechanics is formulated in terms of the longitudinal variation of a single velocity and a single pressure variable, as outlined in the Introduction, this formulation can clearly still incorporate 3D fluid coupling. It may thus be misleading to call this a 1D formulation, even though it does only have one dimension, and so we

have used the more clunky term “uniaxial” to describe this single axis model of the cochlear mechanics.

The long wavelength component of the fluid coupling in the discrete model can be readily calculated using the finite difference approach used by Neely (1981) and Neely and Kim (1986), so that the spatial derivative in equation (2.4) is written as

$$\frac{p_{\mathrm{L}}(n-1)-2p_{\mathrm{L}}(n)+p_{\mathrm{L}}(n+1)}{\Delta^2}=-\frac{2i\omega\rho}{h}v(n). \tag{2.10}$$

The length of one element is denoted Δ and if the first and last elements, representing the boundary conditions at the base and apex, are assumed to have the same length as the BM elements, then $\Delta = L/H$, where L is the assumed length of the cochlea.

The accuracy of this approximation for the long wavelength component of the fluid coupling can be assessed in the wavenumber domain by taking the Fourier transforms of the sequences on both sides of equation (2.10) (Rabiner and Gold, 1975), assuming the effective height is constant, so that

$$\frac{(e^{ik\Delta}-2+e^{-ik\Delta})}{\Delta^2}P(e^{ik\Delta})=-\frac{2i\omega\rho}{h}V(e^{ik\Delta}) \tag{2.11}$$

and so

$$\frac{P(e^{ik\Delta})}{V(e^{ik\Delta})}=\frac{i\omega\rho\Delta^2}{(1-\cos k\Delta)h}. \tag{2.12}$$

This ratio is the fluid coupling impedance corresponding to the finite difference approximation, which can be written in a similar form to equation (2.2) to give the equivalent height in this case as

$$Q_{\mathrm{FD}}(e^{ik\Delta})=\frac{\Delta^2}{2h(1-\cos k\Delta)}. \tag{2.13}$$

In the limit when $k\Delta$ is much less than unity, the series approximation to $\cos k\Delta$ can be used to show that this is equal to $Q_{\mathrm{L}}(k)$ in equation (2.7). The smallest

wavelength that can be unambiguously represented by this discrete formulation is 2Δ, corresponding to a wavenumber of π/Δ. At this wavenumber, $Q_{\mathrm{FD}}(e^{ik\Delta})$ is equal to $\Delta^2/4h$, whereas $Q_{\mathrm{L}}(k)$ in equation (2.7) is equal to $\Delta^2/\pi^2 h$. The finite difference approximation thus overestimates the fluid coupling by a factor of about 2.5 at the smallest wavelengths that can be represented. It provides a good representation of $Q_{\mathrm{L}}(k)$, however, with less than 10% error, when there are at least six elements within the shortest wavelength present, which is the criterion for an accurate discrete representation quoted in the Introduction. Fig. 2.3 shows the finite difference approximation to the long wavelength fluid coupling, equation (2.7), together with the true value equation (2.13) up to *kH* equal to $\pi H/\Delta$.

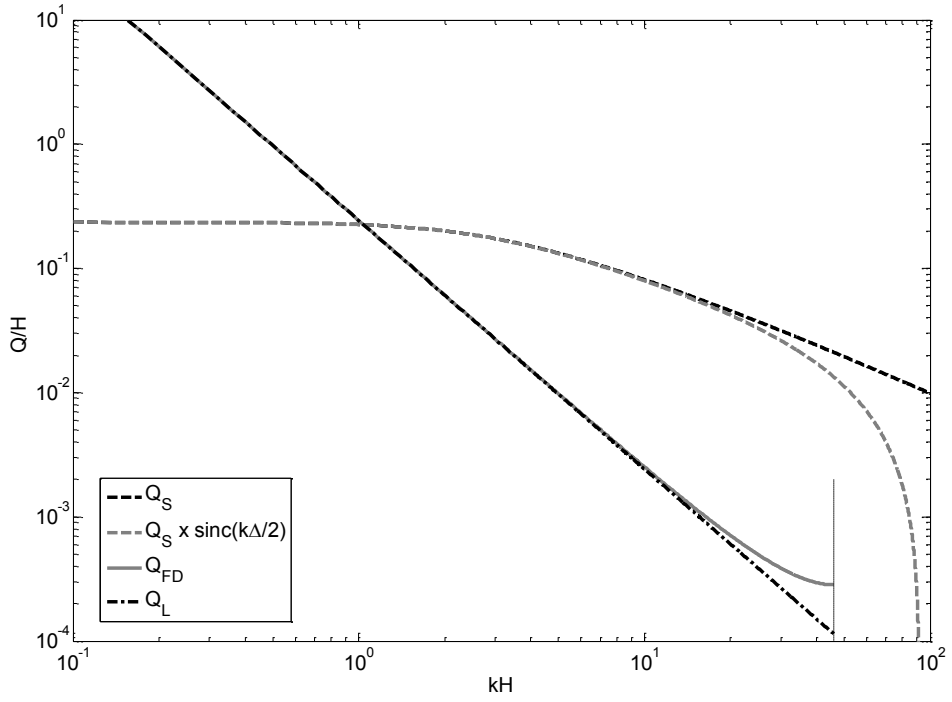

Fig. 2.3 *The wavenumber distribution of the long wavelength component of the normalised fluid coupling impedance, $Q_{\mathrm{L}}(k)$, (dot-dash) and the long wavelength component using the discrete finite difference approximation, Q_{FD} (light solid). Also plotted is the short wavelength component (dashed), together with this multiplied by $\mathrm{sinc}(k\Delta/2)$, to give the wavenumber distribution for this component in the discrete case. The maximum wavenumber that can be represented by the discrete model, for which kH is equal to $\pi H/\Delta$, is indicated by a thin vertical dashed line.*

The boundary conditions at the base and apex of the cochlea are assumed to be determined by the velocity of the stapes, corrected for the difference between the stapes and the chamber area, u_s , and a zero pressure difference condition at the helicotrema, so that

$$\frac{\partial p_L(x)}{\partial x}|_{x=0} = -2i\omega\rho u_s \quad \text{and} \quad p_L(x)|_{x=L} = 0. \tag{2.14, 2.15}$$

In the discrete representation, the finite difference method can be used at the base to express these boundary conditions as

$$\frac{p_L(2) - p_L(1)}{\Delta} = -2i\omega\rho u_s \quad \text{and} \quad p_L(N) = 0. \tag{2.16, 2.17}$$

The complete discrete model of long wavelength fluid coupling can thus be written in matrix form as

$$\frac{1}{\Delta^2}\begin{bmatrix} -\Delta & \Delta & & & & \\ h & -2h & h & & & \\ 0 & h & -2h & h & & \\ & & \ddots & & & \\ & & & h & -2h & h \\ & & & 0 & 0 & \Delta^2 \end{bmatrix}\begin{bmatrix} p_L(1) \\ p_L(2) \\ \\ \vdots \\ p_L(N-1) \\ p_L(N) \end{bmatrix} = -2i\omega\rho\begin{bmatrix} 0 \\ v(2) \\ \\ \vdots \\ v(N-1) \\ 0 \end{bmatrix} - 2i\omega\rho\begin{bmatrix} u_s \\ 0 \\ \\ \vdots \\ 0 \\ 0 \end{bmatrix} \tag{2.18}$$

or, more compactly, as

$$\mathbf{F}\,\mathbf{p}_L = -2i\omega\rho[\mathbf{v} + \mathbf{v}_s], \tag{2.19}$$

so that

$$\mathbf{p}_L = \mathbf{p}_{Ls} + \mathbf{Z}_L\mathbf{v}, \tag{2.20}$$

where $\mathbf{Z}_L$ is equal to $-2i\omega\rho\mathbf{F}^{-1}$ and denotes the long wavelength fluid coupling matrix, and $\mathbf{p}_{Ls}$ is equal to $-2i\omega\rho\mathbf{F}^{-1}\mathbf{v}_s$ and denotes the pressure vector due to the stapes motion.

Taking only the long wavelength components of the fluid coupling into account and using the expression for $\mathbf{Z}_{\mathrm{L}}$ above, equation (1.14) for the vector of pressures in the coupled cochlea can be written as

$$\mathbf{p} = \left[\mathbf{I} - 2i\omega\rho \mathbf{F}^{-1} \mathbf{Y}_{\mathrm{BM}} \right]^{-1} \mathbf{p}_{\mathrm{Ls}} . \tag{2.21}$$

Using the expression for $\mathbf{p}_{\mathrm{Ls}}$ above and the properties of the matrix inverse, this can be written as

$$\mathbf{p} = \left[\mathbf{F} - 2i\omega\rho \mathbf{Y}_{\mathrm{BM}} \right]^{-1} \mathbf{v}_{\mathrm{s}} , \tag{2.22}$$

which is the form of equation originally suggested by Neely (1981) and used by Neely and Kim (1986). The matrix to be inverted in equation (2.22) is tridiagonal, for which the inverse can be efficiently computed, using Gaussian elimination, for example.

Fig. 2.4 illustrates the spatial distribution of this long wavelength pressure difference, proportional to the columns of the matrix $\mathbf{F}^{-1}$, for excitation at a number of different locations along the cochlea. The imaginary component has been plotted for the assumed velocity excitation here and below, but it would be real for an acceleration source. These distributions are very similar to those obtained from an analytic solution to the differential equation for the long wavelength fluid coupling, equation (2.4), with the appropriate boundary conditions, which can be obtained by assuming that $v(x)$ is equal to v_0 between $x_0 - \Delta$ and x_0, and is zero elsewhere, and setting $\partial p_{\mathrm{L}} / \partial x$ equal to the slope of the linear fall off in pressure for x greater than x_0, and is given by

$$p_{\mathrm{L}}(x) = 2i\omega\rho \frac{(L - x_0)}{h} \Delta v_0 \quad \text{for} \quad 0 < x < x_0 - \Delta , \tag{2.23}$$

$$p_{\mathrm{L}}(x) = 2i\omega\rho \frac{(L - x)}{h} \Delta v_0 \quad \text{for} \quad x_0 < x < L , \tag{2.24}$$

where, for continuity, it has been assumed below that Δ is very small compared with L.

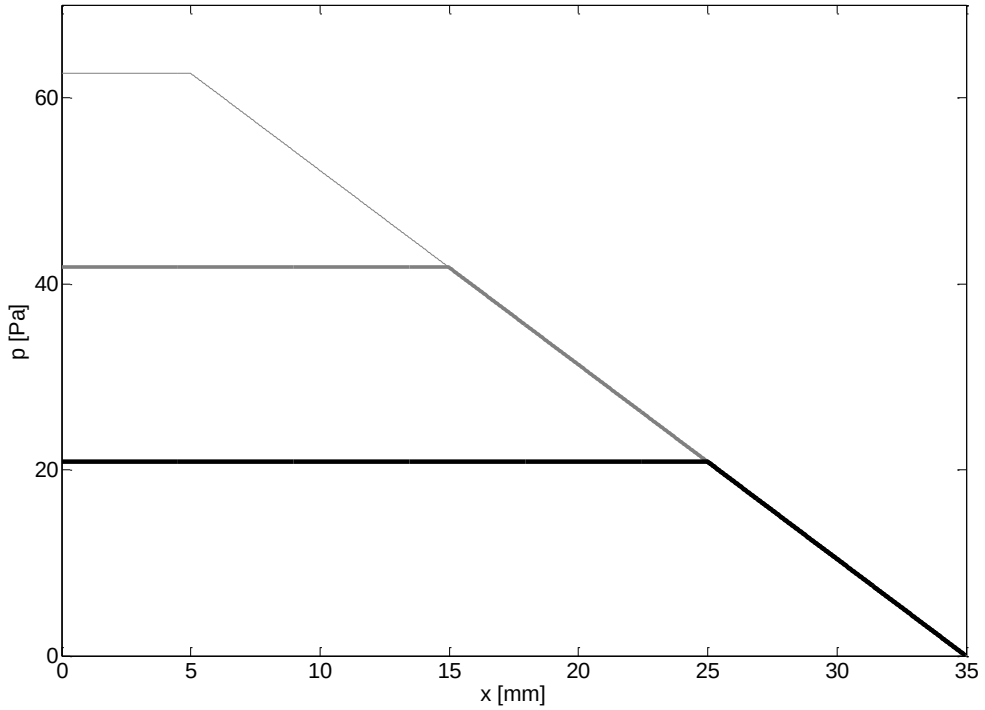

Fig. 2.4 *Distribution of the pressure difference along the cochlea due to the* long wavelength *component of the fluid coupling when only a single element of the discrete BM at x = 5 mm (light line), 15 mm (medium line) or 25 mm (dark line) is driven sinusoidally with a velocity of 10 mm·s^{-1} at a frequency of 1 kHz.*

We now define the full fluid coupling matrix for the discrete model to be

$$\mathbf{Z}_{\mathrm{FC}} = \mathbf{Z}_{\mathrm{L}} + \mathbf{Z}_{\mathrm{S}}, \tag{2.25}$$

where $\mathbf{Z}_{\mathrm{S}}$ contains the terms due to short wavelength coupling. When transformed into the spatial domain, the Fourier transform of $Z_{\mathrm{S}}(k)$ in equation (2.3) contains singularities, due to the implicit assumption of a velocity distribution equal to a spatial delta function. In the discrete model, however, the motion of the *n*-th single BM element represents a finite velocity distribution given by

$$v_n(x) = v(n), \quad \text{for} \quad x = (n-1)\Delta \text{ to } n\Delta, \text{ and zero elsewhere,} \tag{2.26}$$

where $v(n)$ is independent of *x*.

The wavenumber spectrum of this velocity distribution is

$$V_n(k) = v(n)\frac{\sin k\Delta/2}{k\Delta/2}e^{-ik(n-\frac{1}{2})\Delta}. \qquad (2.27)$$

The component of the pressure distribution generated by this velocity distribution due to the short wavelength fluid coupling is then

$$P_n(k) = Z_S(k)V_n(k). \qquad (2.28)$$

The short wavelength component of the fluid coupling in the wavenumber domain, and that multiplied by $\mathrm{sinc}(k\Delta/2)$ are shown in Fig. 2.3.

Equation (2.28) can be numerically evaluated using the above variation for $V_n(k)$ and the fact that $Z_S(k)$ is equal to $Z_{FC}(k)$, derived in the Appendix, minus $Z_L(k)$ defined by equation (2.7). The Fourier transform of equation (2.28) can then be used to calculate the short wavelength component of the pressure in the spatial domain, as shown in Fig. 2.5 for excitation by a single element. Averaging this continuous pressure distribution over each element of the discrete model then provides the discrete pressure distribution due to the short wave coupling, as also shown in Fig. 2.5.

Since the short wavelength component of the fluid coupling impedance is equal to a constant for *kH* less than about unity, as shown in Fig. 2.1, then for such small values of *k*, $Z_S(k)$ can be written as $2i\omega\rho T$, where *T* is an effective fluid thickness, whose variation with *B*/*W* is discussed in the Appendix. The short wavelength pressure contribution, equation (2.28), for $k = 0$, $P_n(0)$, is thus equal to $2i\omega\rho Tv(n)$, where the limiting case of equation (2.27) has also been taken. Using the properties of the wavenumber transform, then $P_n(0)$ is also equal to the integral of the short wavelength component of the pressure in the spatial domain, or, equivalently, to the sum of the elements of the discrete pressure distribution shown in Fig. 2.5. This observation can be used to provide an independent check on the magnitude of the short wavelength components. It also suggests that an approximation to the short wavelength component, which is valid if the wavelength of the slow cochlear wave is long compared with the 1 mm or so range of the short wavelength pressure shown in Fig. 2.5, is a single pressure acting at the point of excitation having a magnitude $2i\omega\rho Tv(n)$. The variable *T* can thus be interpreted as the equivalent thickness of the

fluid loading on the BM due to the nearfield, short wavenumber, components of the pressure (Neely, 1985), further approximations of which are discussed in the Appendix.

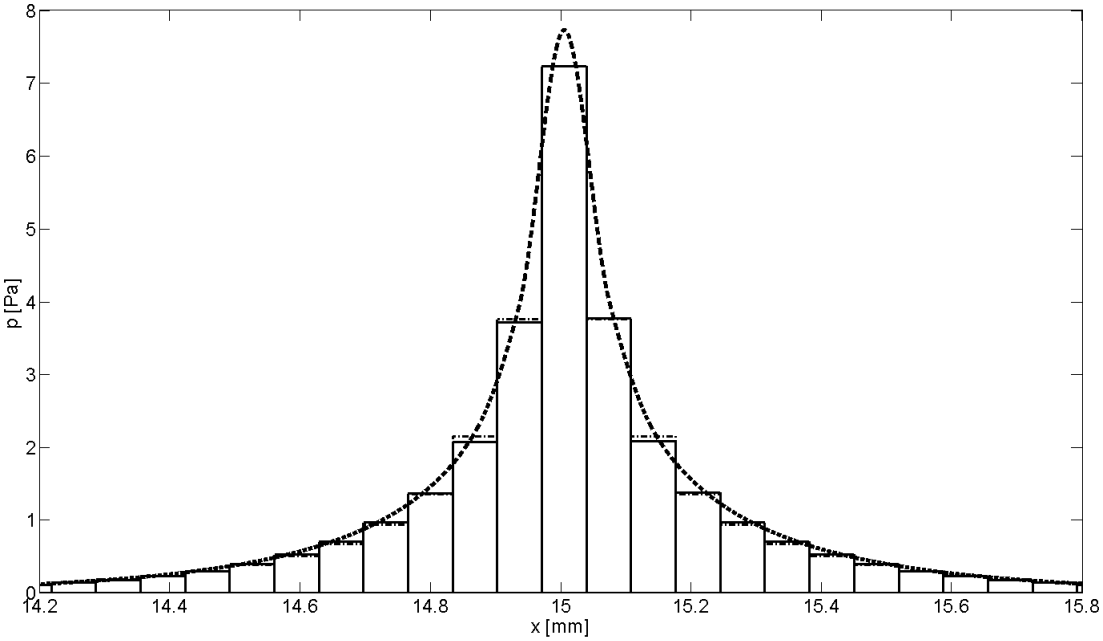

Fig. 2.5 *Distribution of the modal pressure along the cochlea due to* short wavelength *fluid coupling (dashed line) and the average pressure over discrete elements of the BM used to calculate the columns of* $\mathbf{Z}_S$ *(solid line), when excited by a single element at x = 15 mm with a velocity of 10 mm·s*$^{-1}$ *at a frequency of 1 kHz. Also shown is the approximation to the averaged pressure given by equation (2.30) (dot-dashed lines).*

The distribution of the short wavelength component of the fluid pressure can also be derived using an analysis of the acoustic field due to an elemental source in a duct, following Doak (1973), as described in the Appendix. The modal pressure distribution is shown to be due to the contributions from a number of evanescent higher order modes in the duct, whose amplitudes decay exponentially, which can be written as

$$p_S(x) = \sum_{m=1}^{\infty} a_m e^{-r/l_m}, \tag{2.29}$$

where m denotes the order of the mode, a_m is its amplitude, r is equal to $|x - x_0|$ and l_m its characteristic decay length. The characteristics length decreases as the mode order gets higher and so it is the lower order modes that dominate when some distance from the source.

In fact, a reasonable approximation to the averaged near field pressure in the discrete model, due to a single BM element, is obtained using only two terms of such a series, so that

$$p_{\mathrm{SA}}(n') = \left(Z_1 e^{-n'\Delta/l_1} + Z_2 e^{-n'\Delta/l_2} \right) v_0, \tag{2.30}$$

where n' is equal to the number of elements from the position where the averaged pressure is evaluated to the exciting element, and is equal to $|n - n_0|$ for excitation of the n_0-th element, Δ is the length of one element and l_1 and l_2 are characteristic decay lengths. The near field pressure amplitudes are proportional to the impedance Z_1 and Z_2, to the n_0-th excitation velocity, $v(n)$ in equation (2.26) and the effective fluid thickness, T. This approximation to the average pressure over the discrete elements is also shown in Fig. 2.5, with Z_1 and Z_2 equal to 201 Pa·s·m^{-1} and 522 Pa·s·m^{-1}, l_1 equal to H/3.47 and l_2 equal to H/12.8, and is seen to provide a good approximation to the result obtained from the inverse Fourier transform of equation (2.28).

A position-shifted sequence of these pressure distributions, normalised by the velocities of each element, can then be used to define the columns of the matrix $\mathbf{Z}_{\mathrm{S}}$, which determines the fluid coupling due to the short wavelength components in the discrete model. The total distributions due to both long- and short wavelength fluid coupling are then obtained by summing these two contributions, as illustrated in Fig. 2.6. These distributions are similar to those shown by other authors, for example Pathasarathi *et al.* 2000, except that the singularity induced by assuming that the velocity is concentrated at a single point has been removed by assuming a finite value of the velocity distribution over the length of an element.

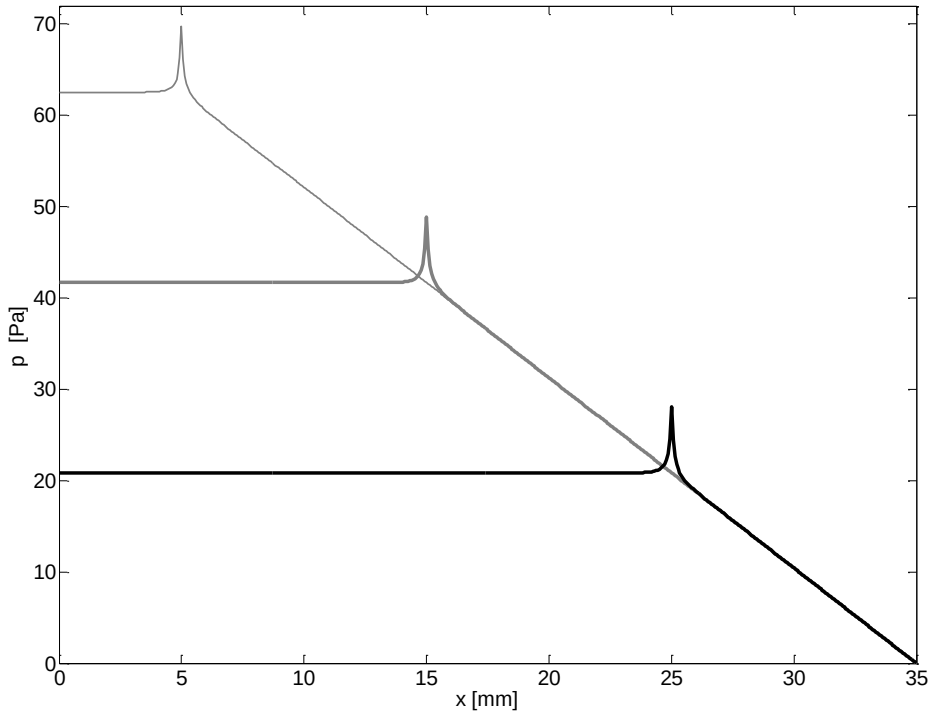

Fig. 2.6 *Distribution of the* total *pressure difference due to both long and short wavelength components in the fluid coupling matrix along the length of the cochlea due to excitation of a single element on the BM at x = 5 mm, 15 mm and 25 mm with a velocity of 10 mm·s^{-1} at a frequency of 1 kHz.*

Although only the pressure *difference* across the BM can drive it into motion, there will also generally be a common-mode component to the pressure distribution in the cochlea, as introduced in Section 1, so that, reiterating equations (1.4, 1.5), the pressure distribution in the two chambers can be written as

$$p_1(x) = p_M(x) + p(x)/2, \tag{2.31}$$

$$p_2(x) = p_M(x) - p(x)/2, \tag{2.32}$$

where $p(x)$ is the complex pressure difference at a given frequency, as above, and $p_M(x)$ is the common-mode pressure distribution. If the fluid is incompressible, the common-mode pressure is uniform throughout the cochlea, and is generally referred to as the mean pressure, which can be written as simply p_M, with no longitudinal dependence.

Peterson and Bogert (1950) argue that the magnitude of p_M is determined by the boundary condition at the round window. If, as assumed by Peterson and Bogert, the

round window is sufficiently flexible that it provides a pressure release boundary condition, then

$$p_2(0) = 0 \quad \text{and so} \quad p_M(x) = p(0)/2. \tag{2.33a,b}$$

This equation, together with the variation of pressure difference shown in Fig. 2.6, allows the individual pressures in the two cavities to be calculated using equations (2.31) and (2.32), which are plotted in Fig. 2.7.

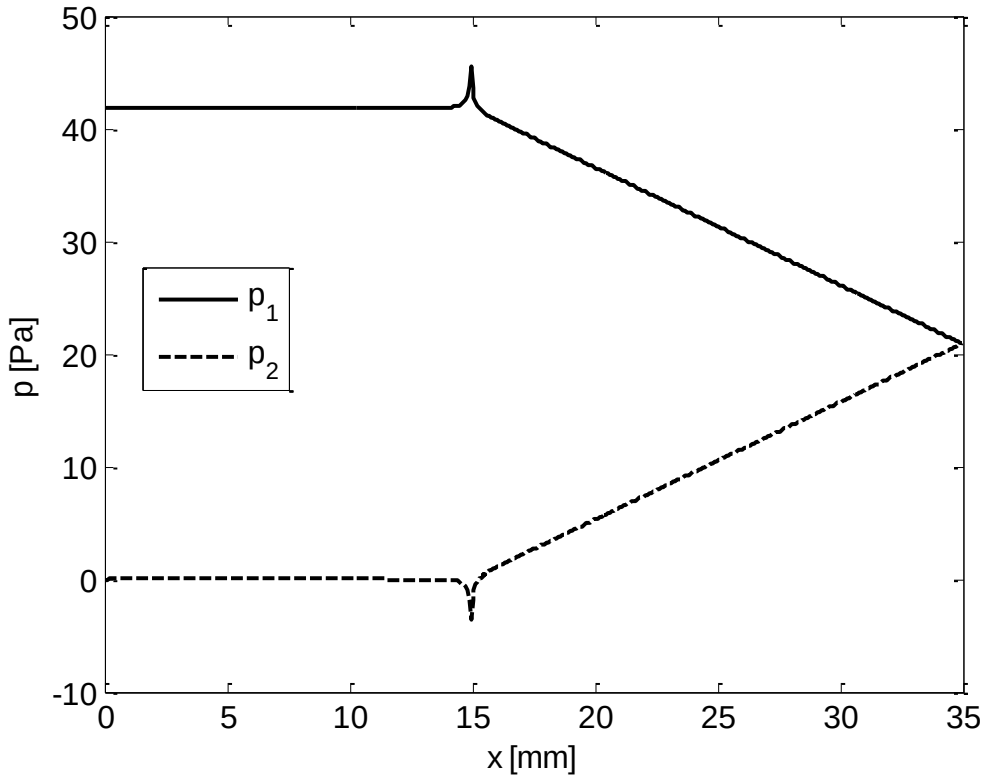

Fig. 2.7 *The individual pressures in the upper and lower cavities along the cochlea, $p_1(x)$ and $p_2(x)$, due to excitation of a single element of the BM at x=* 15 mm *with a velocity of 10 mm·s^{-1} at a frequency of 1 kHz.*

It should be noted that these distributions of the individual pressures are considerably simpler than those shown by Peterson and Bogert (1950), since they are generated here by the motion of a single element along the BM, whereas Peterson and Bogert calculate the solution for the coupled problem where the whole BM interacts with the fluid. The BM motion has a considerably more complicated form in the coupled case, and includes phase variations along the length of the cochlea that are not present in either the pressure difference or the mean pressure calculated here.

In Fig. 2.7 we have assumed a perfect equalisation of the two pressures at the helicotrema, due to it having a zero impedance, but in practice a pressure difference of $p(L)$ will exist, due to a finite helicotrema impedance

$$\frac{p(L)}{v(L)} = Z_{\mathrm{H}}, \tag{2.34}$$

where $v(L)$ is the transverse velocity through the helicotrema. Assuming that the pressure difference is dominated by long wavelength components at the helicotrema, the transverse velocity at the helicotrema is related to the longitudinal velocity, $u(x)$, by the continuity equation

$$\frac{\partial u(x)}{\partial x} = \frac{v(x)}{h}, \tag{2.35}$$

so that if $u(x)$ is proportional to $e^{i(\omega t - kx)}$, then

$$v(L) = -ikhu(L). \tag{2.36}$$

The longitudinal velocity is related to the pressure distribution for a 1D fluid flow by the momentum equation

$$\frac{\partial p(x)}{\partial x} = -2\rho \frac{\partial u(x)}{\partial t}, \tag{2.37}$$

so that

$$u(L) = -\frac{1}{2i\omega\rho} \frac{\partial p(x)}{\partial x}\Big|_{x=L}, \tag{2.38}$$

and the pressure difference at the helicotrema is

$$p(L) = Z_{\mathrm{H}} v(L) = Z_{\mathrm{H}} \frac{kh}{2\omega\rho} \frac{\partial p(x)}{\partial x}\Big|_{z=L}. \tag{2.39}$$

Differentiating equation (2.24) for the pressure distribution gives

$$\frac{\partial p(x)}{\partial x}\Big|_{x=L} = -\frac{2i\omega\rho}{h} \Delta v_0(x_0), \tag{2.40}$$

for the pressure gradient due to excitation of a single BM element with velocity $v_0(x_0)$ at position x_0 but since equation (2.40) does not depend on x_0 this can be written just as v_0. The helicotrema pressure difference in this case is thus

$$p(L) = -iZ_{\mathrm{H}} k\Delta\, v_0, \tag{2.41}$$

and generally this pressure difference is proportional to the sum of all the elemental BM velocities.

Assuming that the frequency is high enough for the BM to be mass dominated at the apex, then the wavenumber at the helicotrema is equal to

$$k = k(L) = \sqrt{\frac{2\rho}{hm(L)}}, \tag{2.42}$$

where $m(x)$ is the mass per unit area of the BM at the apex. Also assuming that the helicotrema impedance is dominated by the mass per unit length of the fluid within it, m_{H}, then

$$Z_{\mathrm{H}} = i\omega m_{\mathrm{H}}. \tag{2.43}$$

Further assuming m_{H} is equal to ρT_{H} and that $m(L)$ is equal to ρT_{BM}, where T_{H} and T_{BM} are the effective thicknesses of the helicotrema and BM, then

$$p(L) \approx \omega\rho\sqrt{\frac{2T_{\mathrm{H}}^2}{hT_{\mathrm{BM}}}}\Delta v_0. \tag{2.44}$$

Assuming that both T_{H} and T_{BM} are 50 μm and h is 4.1 mm, this pressure is about 0.7 μPa for a BM velocity of 10 mms^{-1} at 1 kHz and so is small compared with the pressure difference in Fig. 2.6, as expected. In practice, there will also be some damping due to viscosity in addition to the mass of the fluid in the helicotrema.

In order to account for a finite value of the helicotrema impedance in the matrix formulation of Section 1, an additional term must be added to all the elements of $\mathbf{Z}_{\mathrm{FC}}$ in equation (1.10) equal to $-iZ_{\mathrm{H}} k\Delta$.

3. Effect of short wavelength fluid coupling on predicted BM distribution

Fig. 3.1 shows a comparison of the predicted BM velocity in a uniform cochlea model having the properties listed in Table 2.1, with either 1D or 3D fluid coupling. In these models the BM mass per unit area has been assumed constant along the length of the cochlea, for simplicity. Its stiffness and damping have been adjusted to achieve an exponential distribution of natural frequency and a constant damping ratio. The value of the BM mass varies, however, between the models using 1D and 3D fluid coupling, since in the former case this must include the added mass due to the nearfield fluid loading, whereas in the latter case this is automatically included. The physical height of the fluid chamber is used in the 3D model, so that the effective chamber height is the same in both cases. These changes, which are similar to those assumed by de Boer (1996) in his "matched" model, for example, are made in order for the results using the 1D and 3D fluid coupling to be as consistent as possible, so that the effects of the fluid coupling can be seen most clearly. A discrete formulation of the fluid coupling and isolated BM dynamics is used, combined using the matrix method described in Section 1.

Although a reasonable matching of the magnitudes can be obtained between 1D and 3D models, the roll-off of the model with 3D fluid coupling is somewhat greater than that of the model with 1D fluid coupling. The accumulation of phase lag of the 1D model, however, is significantly less than that of the 3D model apical to the characteristic place as also observed by de Boer (1996) and Kolston (2000). This reflects the changes in the wavelength of the BM motion as it approaches the characteristic place, becoming comparable with the chamber height and invalidating the assumptions of the 1D model. There is then a reduction in longitudinal fluid flow and an increase in the local mass loading, slowing the wave and increasing the phase accumulation (Kolston, 2000).

The source of the ripples in the response calculated with the 3D fluid coupling is not clear. They do not appear to be the result of numerical discretisation errors, since their form is almost unchanged if the number of elements is doubled. They are, however, reminiscent of the notches noted in numerical solutions of BM velocity with higher

order fluid coupling by de Boer and Viergever (1982) and Watts (2000) and attributed to multiple wave propagation by these authors.

The accumulated phase lag at the characteristic place for a model with only long wavelength fluid coupling and passive, single degree of freedom, BM mechanics with very little damping (Schroeder, 1973; Zweig *et al.*, 1976) is

$$\phi_n \approx \frac{\pi l}{2d} \text{ radians} = \frac{l}{4d} \text{ cycles}, \tag{3.1}$$

where l is the assumed exponential length scale of the characteristic frequency along the cochlea, which is about 7 mm for humans, as assumed here, and d is a characteristic distance that relates the fluid coupling and BM mass given by

$$d = \sqrt{\frac{hm_0}{2\rho}}, \tag{3.2}$$

which for the parameters assumed here is about 0.77 mm. The predicted phase lag at the characteristic place is about 2.3 cycles, which is somewhat greater than the phase shift at the positions where the BM velocity is greatest in Fig. 3.1, due to the effects of damping, but is reasonable agreement with the asymptotic phase shift for the 1D model. It is clear, however, that this estimate of accumulated phase is not appropriate for the case with 3D fluid dynamics.

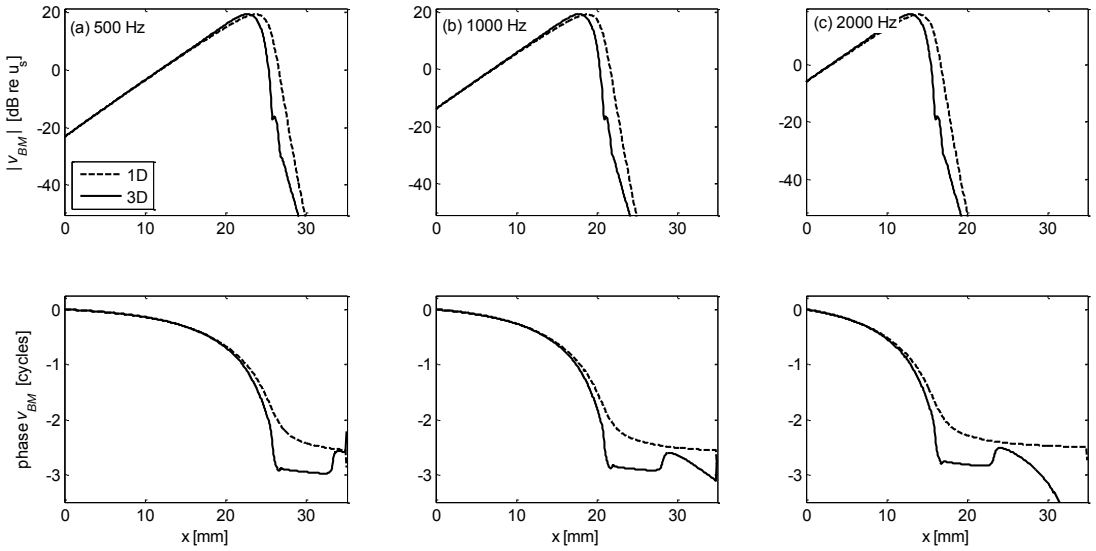

Fig. 3.1 *BM velocity, normalised to that of the stapes for the coupled model with either full 3D fluid coupling and a BM mass of 0.05 kg·m^{-2} or 1D fluid coupling and a BM mass of 0.29 kg·m^{-2}, with excitation frequencies of (a) 500 Hz, (b) 1 kHz and (c) 2 kHz.*

4. Pressure difference and mean pressure in an asymmetric and non-uniform cochlea

In this Section a one-dimensional analysis is used to derive the long wavelength component of the pressure in each of the fluid chambers for a model of the cochlea with asymmetrical and non-uniform fluid chambers and hence the long wavelength contribution to the pressure difference and mean pressure. Since the short wavelength components of the pressure are not significantly affected by the shape of the cochlear chambers, they will continue to be approximately equal and opposite in the two chambers and can be calculated using the wavenumber approach for a uniform cochlea described above. An example is then given of the calculated pressure difference and mean pressure for two assumed variations of the chamber volumes. The effect of this modified fluid coupling on the coupled response of the passive cochlear model is then illustrated.

If areas of the upper fluid chamber (SM and SV) and the lower fluid chamber (ST) vary along the length of the cochlea as $A_1(x)$ and $A_2(x)$, the long wavelength component of the pressure will be determined by the continuity and momentum equations. Assuming that the longitudinal fluid velocity in a single chamber, averaged across its cross-sectional area, is $\bar{u}(x)$, and that the transverse BM velocity averaged across the width of the chamber is $\bar{v}(x)$, then the continuity equation for this chamber can be written as

$$\frac{\partial}{\partial x}(A(x)\bar{u}(x)) = W(x)\bar{v}(x), \tag{4.1}$$

where in general the BM width also varies along the cochlear as $W(x)$. This is equivalent to the equation used by Peterson and Bogert (1950), except that the fluid is assumed here to be incompressible.

The momentum equation can also be written in terms of the complex pressure averaged across the cross-sectional area, $\bar{p}(x)$, as

$$\frac{\partial \bar{p}(x)}{\partial x} = -i\omega\rho\bar{u}(x). \tag{4.2}$$

Substituting $\bar{u}(x)$ in equation (4.2) into equation (4.1) gives an expression for $\bar{p}(x)$ in terms of $\bar{v}(x)$ as

$$\frac{\partial}{\partial x}\left(A(x)\frac{\partial \bar{p}(x)}{\partial x} \right) = -i\omega\rho W(x)\bar{v}(x), \tag{4.3}$$

which is an incompressible form of Webster's horn equation, described by Fletcher and Rossing (1998), for example.

We now assume that W is independent of x, although only minor modifications to the analysis are required to incorporate this dependence. Applying equation (4.3) to the upper chamber, it can be written in terms of the modal BM velocity, $v(x)$, and the modal pressure $p_1(x)$, by noting that the velocity distribution in the radial direction at position x is equal to $v(x)\ \psi(y)$, so that

$$\bar{v}(x) = \frac{v(x)}{W}\int_0^W \psi(y)dy, \tag{4.4}$$

and since, in the long wavelength limit, the pressure is uniform over the BM, then the definition of the modal pressure gives

$$p_1(x) = \frac{\bar{p}(x)}{W}\int_0^W \psi(y)dy. \tag{4.5}$$

If the BM velocity is a half sinusoid over a distance B on one side of the fluid chamber, as assumed in the Appendix, then in this case

$$\frac{1}{W}\int_0^W \psi(y)dy = \frac{2}{\pi}\sqrt{\frac{2B}{W}}. \tag{4.6}$$

The long wavelength fluid coupling equation in the upper chamber can thus be written in terms of the modal pressure, and modal velocity as

$$\frac{\partial}{\partial x}\left[A_1(x)\frac{\partial}{\partial x}\left(\frac{p_1(x)}{\sqrt{B(x)}} \right) \right] = -\frac{8i\omega\rho}{\pi^2}v(x)\sqrt{B(x)}. \tag{4.7}$$

If B were independent of x, this could be written as

$$\frac{\partial}{\partial x}\left(h_1(x)\frac{\partial p_1(x)}{\partial x} \right) = -i\omega\rho v(x), \tag{4.8}$$

where $h_1(x)$ is the effective height of the upper chamber, which is equal to

$$h_1(x) = \frac{\pi^2 A_1(x)}{8B}, \tag{4.9}$$

in agreement with the limiting case of the wavenumber analysis presented in the Appendix.

In general, however, the in the lower fluid chamber is similarly related to the modal BM velocity by

$$\frac{\partial}{\partial x}\left[A_2(x)\frac{\partial}{\partial x}\left(\frac{p_2(x)}{\sqrt{B(x)}} \right) \right] = \frac{8i\omega\rho}{\pi^2} v(x)\sqrt{B(x)}. \tag{4.10}$$

The integral of $i\omega\rho v(x)$ with respect to x is thus equal to both of the expressions below

$$\frac{8i\omega\rho}{\pi^2}\int_0^x v(x')\sqrt{B(x')}dx' = A_2(x)\frac{\partial}{\partial x}\left(\frac{p_2(x)}{\sqrt{B(x)}} \right) = -A_1(x)\frac{\partial}{\partial x}\left(\frac{p_1(x)}{\sqrt{B(x)}} \right), \tag{4.11}$$

where the fact that both $\partial p_1(x)/\partial x$ and $\partial p_2(x)/\partial x$ are zero when x is equal to zero has been used to eliminate any constants of integration. The pressure gradients in the two chambers are thus related by

$$\frac{\partial}{\partial x}\left(\frac{p_2(x)}{\sqrt{B(x)}} \right) = -\frac{A_1(x)}{A_2(x)}\frac{\partial}{\partial x}\left(\frac{p_1(x)}{\sqrt{B(x)}} \right). \tag{4.12}$$

We can relate the long wavelength component of the modal pressure difference, $p_L(x)$, to the modal BM velocity, $v(x)$, via the equivalent area $A_d(x)$ in the expression

$$\frac{\partial}{\partial x}\left[A_d(x)\frac{\partial}{\partial x}\left(\frac{p_L(x)}{\sqrt{B(x)}}\right)\right]=-\frac{16i\omega\rho}{\pi^2}v(x)\sqrt{B(x)}, \tag{4.13}$$

where $p_L(x)$ is equal to $p_1(x) - p_2(x)$. The integral in equation (4.11) is thus also equal to

$$\frac{8i\omega\rho}{\pi^2}\int_0^x v(x')\sqrt{B(x')}dx' = -\frac{A_d(x)}{2}\left[\frac{\partial}{\partial x}\left(\frac{p_1(x)}{\sqrt{B(x)}}\right)-\frac{\partial}{\partial x}\left(\frac{p_2(x)}{\sqrt{B(x)}}\right)\right]. \tag{4.14}$$

Using equation (4.12) and equating (4.14) to the final form of equation (4.11) allows the equivalent area for the pressure difference to be written (Zwislocki, 1953) as

$$A_d(x)=\frac{2A_1(x)A_2(x)}{A_1(x)+A_2(x)}. \tag{4.15}$$

Similarly, the component of the mean pressure p_m(x), equal to $\left[p_1(x)+p_2(x)\right]/2$, due to the asymmetry of the cochlear chambers obeys the equation

$$\frac{\partial}{\partial x}\left[A_m(x)\frac{\partial}{\partial x}\left(\frac{p_L(x)}{\sqrt{B(x)}}\right)\right]=-\frac{16i\omega\rho}{\pi^2}v(x)\sqrt{B(x)}, \tag{4.16}$$

where

$$A_m(x)=\frac{4A_1(x)A_2(x)}{A_2(x)-A_1(x)}. \tag{4.17}$$

An analytic solution to the pressure difference can be obtained for excitation of a single BM element, having a velocity of v_0 from $x_0-\Delta$ to x_0, by integrating equation (4.13) and using the boundary condition that $\partial p_L(x)/\partial x$ is zero and assuming that $B(x)$ is independent of x at $x = 0$ to give

$$\frac{\partial}{\partial x}\left(\frac{p_L(x)}{\sqrt{B(x)}}\right)=0, \qquad 0<x<x_0-\Delta, \tag{4.18}$$

$$\frac{\partial}{\partial x}\left(\frac{p_L(x)}{\sqrt{B(x)}}\right) = -\frac{16i\omega\rho\Delta v_0\sqrt{B(x)}}{\pi^2 A_d(x)}v(x) \qquad x_0 < x < L. \qquad (4.19)$$

The boundary condition that $p_L(x)$ is zero at $x = L$ and the fact that Δ is small compared with L can then be used to integrate these expressions again to give the pressure distribution of long wavelength pressure difference as

$$p_L(x) = -16i\omega\rho\Delta v_0\sqrt{B(x_0)B(x)}\int_{x_0}^{L}\frac{1}{A_d(x')}dx', \qquad 0 < x < x_0 - \Delta, \qquad (4.20)$$

$$p_L(x) = -16i\omega\rho\Delta v_0\sqrt{B(x_0)B(x)}\int_{x}^{L}\frac{1}{A_d(x')}dx', \qquad x_0 < x < L. \qquad (4.21)$$

Similar expressions can be derived for the mean pressure in equation (4.16).

If the areas of the fluid chambers in the cochlear models are divided up into N discrete sections, as for the BM, equations (4.8), (4.10) and (4.15) can be used to calculate the equivalent area for the pressure difference at the nth discrete element as $A_d(n)$. The integrals in equations (4.20) and (4.21) can then be approximated by summations to give the pressure at the nth element as

$$p_L(n) = -16i\omega\rho\Delta^2 v_0\sqrt{B(n_0)B(n)}\sum_{n'=n_0}^{N}\frac{1}{A_d(n')}, \qquad 0 < n < n_0 - 1, \qquad (4.22)$$

$$p_L(n) = -16i\omega\rho\Delta^2 v_0\sqrt{B(n_0)B(n)}\sum_{n'=n}^{N}\frac{1}{A_d(n')}, \qquad n_0 < n < N, \qquad (4.23)$$

where $n_0 = x_0/\Delta$.

Alternatively, the full matrix of long wavelength fluid coupling impedances can be calculated by using a generalisation of Neely's finite difference method. Differentiating equation (4.13) by parts, in the case it is assumed that there is no variation of B with x, gives

$$h_d(x)\frac{\partial^2 p_L(x)}{\partial x^2} + \frac{\partial h_d(x)}{\partial x}\frac{\partial p_L(x)}{\partial x} = -2i\omega\rho v(x). \qquad (4.24)$$

where h_d is equivalent height and given by

$$h_d(x) = \frac{h_1(x)h_2(x)}{2(h_1(x)+h_2(x))}. \tag{4.25}$$

Approximating $\partial^2 p_L(x)/\partial x^2$ as in equation (2.10), using the boundary conditions in equations (2.16) and (2.17), and now taking the finite difference approximation

$$\frac{\partial h_d(x)}{\partial x}\frac{\partial p_L(x)}{\partial x} = \frac{1}{\Delta^2}\big(h(n+1)-h(n)\big)\big(p_L(n+1)-p_L(n)\big), \tag{4.26}$$

allows the complete described model of fluid coupling to be written, by analogy with equation (2.19), as

$$(\mathbf{F}_1+\mathbf{F}_2)\mathbf{p}_L = -2i\omega\rho(\mathbf{v}+\mathbf{v}_s), \tag{4.27}$$

where now

$$\mathbf{F}_1 = \frac{1}{\Delta^2}\begin{bmatrix} -\Delta & \Delta & 0 & \cdots & & & \\ h_d(2) & -2h_d(2) & h_d(2) & & & & \\ 0 & h_d(3) & -2h_d(3) & h_d(3) & & & \\ & & \ddots & \ddots & & & \\ & & & h_d(N-1) & -2h_d(N-1) & h_d(N-1) & \\ & & & 0 & 0 & \Delta^2 & \end{bmatrix} \tag{4.28}$$

and

$$\mathbf{F}_2 = \frac{1}{\Delta^2}\begin{bmatrix} (h_d(1)-h_d(2)) & (h_d(2)-h_d(1)) & & \cdots & & \\ 0 & (h_d(2)-h_d(3)) & (h_d(3)-h_d(2)) & & & \\ & & \ddots & \ddots & & \\ & & & & (h_d(N-1)-h_d(N)) & (h_d(N)-h_d(N-1)) \\ & & & & 0 & 0 \end{bmatrix}. \tag{4.29}$$

Fig. 4.1 shows an assumed variation of A_1 and A_2 along the length of the human cochlea, together with corresponding assumed variations in the width of the fluid

chamber, *W*, and BM width, *B*. These are based on the areas in the cross sectional figures published by Zakis and Witte (2001), which are interpolated using a cubic spline function. They are reasonably consistent with the measurements of Thorne et al (1999) and the earlier estimates shown in Fig. 79 of Fletcher (1953) and Fig. 4.5 in Zwislocki (2002). The equivalent heights for the two fluid chambers calculated from equations (4.8) and (4.10) and the effective heights for the pressure difference and mean pressure, equations (4.15) and (4.17) are also shown in Fig. 4.1. The equivalent height for the mean pressure is significantly larger than that for the pressure difference since the difference between the areas of the two chambers is small compared with their average value. The equivalent height for the mean pressure also changes sign about 33 mm along the cochlea since at this point A_1 becomes greater than A_2.

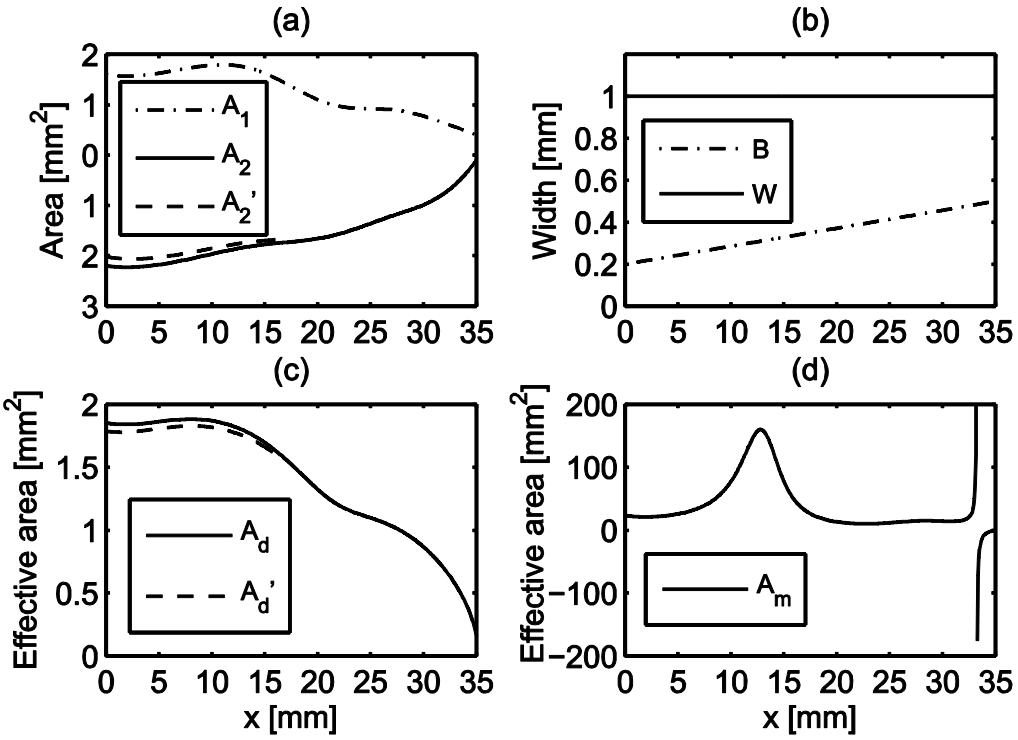

Fig. 4.1 *The first assumed variation in (a) the area of the upper, A_1, and lower, A_2, fluid chambers as a function of longitudinal position in the asymmetric model, together with (b) the assumed variation in the width of the cochlear partition, W, and BM width, B, (c) the calculated effective area for the pressure difference and (d) the calculated effective area for the mean pressure A_m. Note that A_m becomes negative for x equal to about 33 mm. The dashed line for A_2 shows the modified area, A_2', and corresponding area A_m' if a short cochlea implant is introduced into the lower chamber, having a length of 16 mm and an area tapering from 0.18 mm^2 to 0.07 mm^2.*

Equations (4.22) and (4.23) can be used to calculate the long wavelength contribution to the pressure difference in the non-uniform cochlea and a similar expression can be used to calculate the mean pressure variation due to asymmetry in two fluid chambers. Although the short wavelength component is assumed to be unaffected by the size of the fluid chambers, it will depend on the proportion of the chamber width occupied by the BM. The variation of the short wavelength component with the ratio B/W is illustrated in Fig.A.4, although there is not much variation over the range $B/W = 0.2$ to $B/W = 0.5$, as required in this case. The distribution of modal pressure difference with both long and short wave components, due to BM excitation by a single element of the BM at 5 mm, 15 mm or 25 mm is shown in Fig. 4.2(a), with the corresponding mean pressure distributions in Fig. 4.2(b). The curvature in the pressure difference distribution for x greater than x_0 is due to the reduction of the equivalent height with distance, as shown in Fig. 4.1(d), and also seen in Fig. A1 of Shera *et al.* (2004), for example, which was calculated using a Green's function approach.

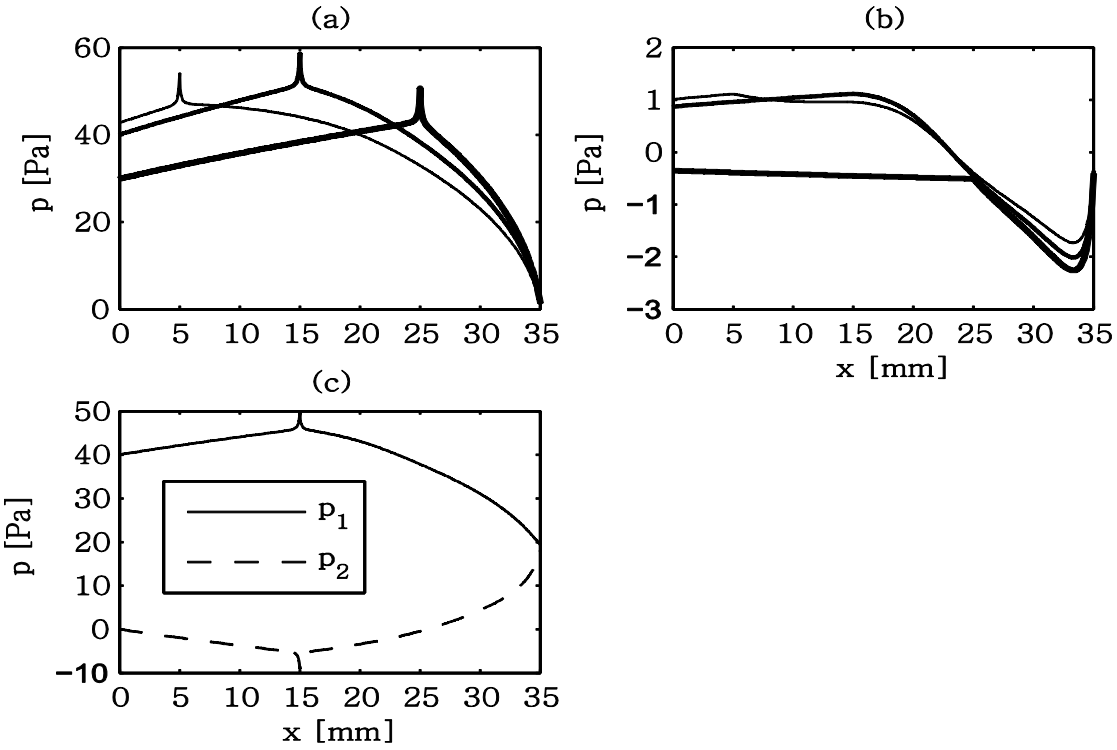

Fig. 4.2 *The calculated total variation in the modal pressure difference (a) due to both long and short wavelength components for the model of the first asymmetrical cochlea, (b) the calculated mean pressure due to the difference in chamber areas when only a single element of the discrete BM at x = 5 mm, 15 mm or 25 mm is driven sinusoidally with a velocity of 10 mm·s^{-1} at a frequency of 1 kHz. Also shown (c) are the pressures in the two individual chambers when only the element at x=15mm is excited.*

Fig. 4.3 shows the calculated distribution of BM velocity calculated by combining the results shown in Fig. 4.2 (c) for the fluid coupling term with the passive BM dynamics along the length of the cochlea in the discrete model. These coupled responses do not, however, look significantly different from those shown in Fig. 3.1 for the uniform cochlea. The dashed lines in Figs. 4.1 show the corresponding area functions and cochlear responses if a short cochlea implant, having a length of 16 mm with an area tapering from 0.18 mm^2 down to 0.07 mm^2, is introduced into the lower chamber. These dimensions are based on the Cochlear Hybrid™ implant (Cochlea, 2008). This small change in area has a negligible effect on the passive behaviour of the cochlear model and the results with and without the implant in Fig. 4.3 cannot be distinguished. The area of the implant needs to be made about ten times larger than that assumed above for the response to change by 1 dB, and this change then only occurs for the response at 2 kHz, whose characteristic place is closest to the end of the implant.

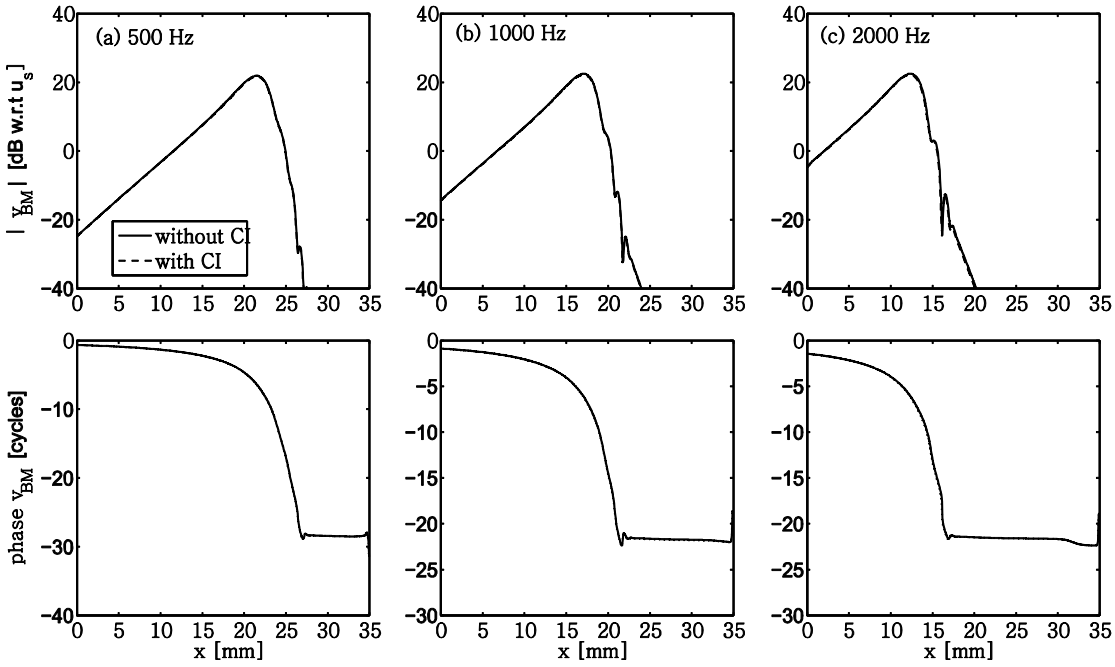

Fig. 4.3 *Coupled BM velocity distribution in the model of the non-uniform cochlea at excitation frequencies of 500 Hz, 1 kHz and 2 kHz. Although the results are shown with and without the effects of the short cochlear implant, the results cannot be distinguished on the scale of this graph.*

The mean pressure shown in Fig 4.2 (b) is significantly less than the pressure difference, since the difference in the effective areas of the two chambers is significantly less than their average value. The effect of this additional component of

mean pressure on the distributions of the pressures in the individual fluid chambers, as shown for the uniform cochlea in Fig. 2.7, is to generate a small asymmetry in the two pressures near the apex, as shown in Fig 4.2 (c).

The effect of this spatially-varying component of the mean pressure is more significant in the case of the guinea pig, for example, since according to the data presented by Fernandez (1952), the difference between the areas of the two chambers at the base of the cochlea is comparable with their average value. This data has been used to generate a second example of an assumed area and BM width variation, as shown in Fig. 4.4. Fig. 4.5 shows the resulting distributions of pressure difference, mean pressure and the pressures in the two chambers in this second case. The component of the mean pressure due to the asymmetry is now more comparable with the pressure difference, causing a clear asymmetry in the pressures in the two chambers.

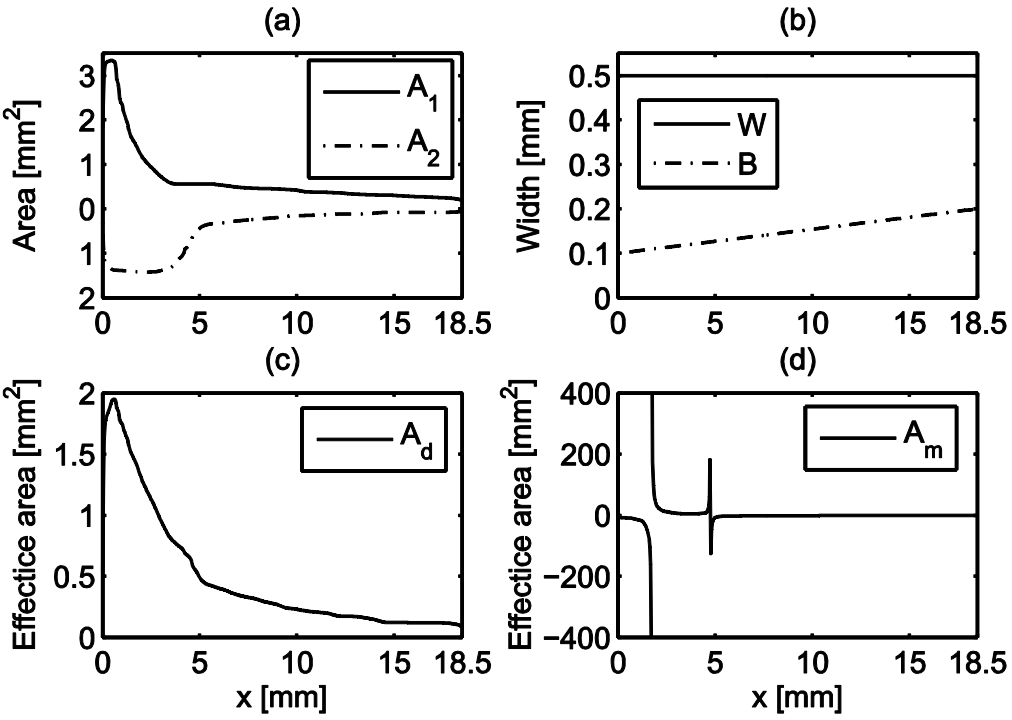

Fig. 4.4 *The second assumed variation in (a) the area of the upper, A_1, and lower, A_2, fluid chambers as a function of longitudinal position in the asymmetric model, together with (b) the assumed variation in the width of the cochlear partition, W, and BM width, B, (c) the calculated effective area for the pressure difference, A_d, and (d) the calculated effective area for the mean pressure, A_m.*

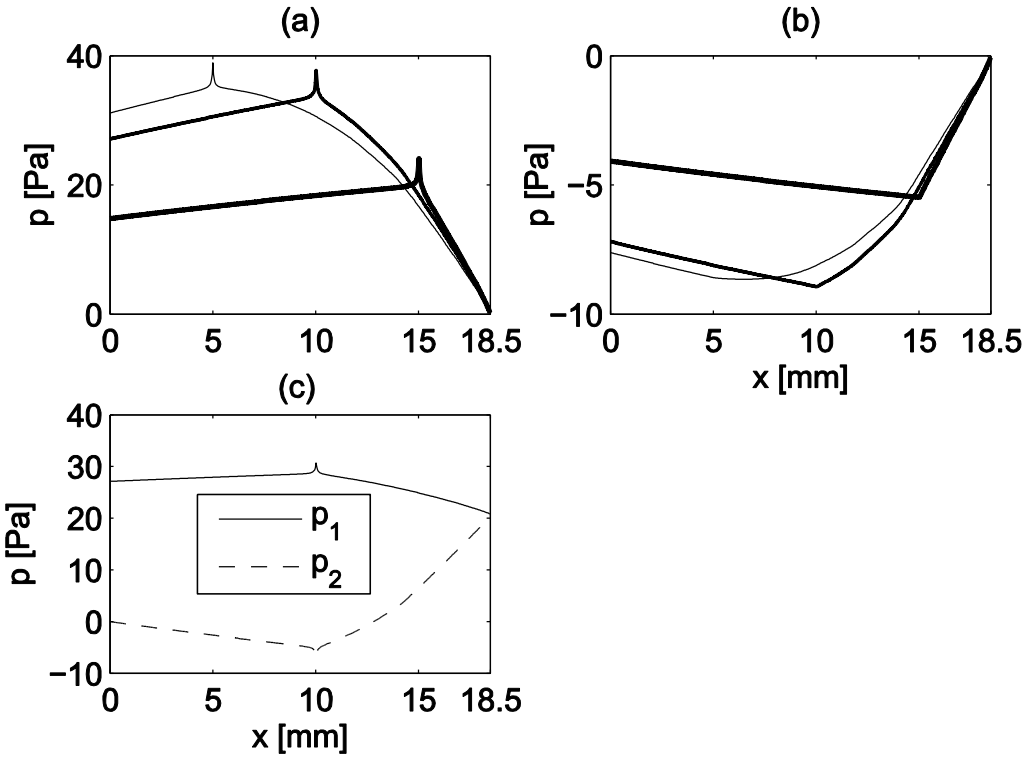

Fig. 4.5 *The calculated total variation in the modal pressure difference for the second example of an asymmetrical cochlea (a) due to both long and short wavelength components, (b) the calculated mean pressure due to the difference in chamber areas when only a single element of the discrete BM at x = 5 mm, 10 mm or 15 mm is driven sinusoidally with a velocity of 10 mm·s^{-1} at a frequency of 1 kHz. Also shown (c) are the pressures in the two individual chambers when only the element at x=15 mm is excited.*

5. Finite element model of fluid coupling

In order to compare the fluid coupling impedances derived above with those derived using an alternative method, a finite element (FE) model of the fluid coupling has been constructed. As well as providing an independent check of the behaviour of the fluid coupling in the uncoiled rectangular box model of the cochlea used above, the finite element model has the advantage that more complicated and realistic geometries can also be analysed.

The finite element model assumes a rigid walled enclosure within which the BM has an imposed velocity contained in the vector $\mathbf{q}_{FE}$, having dimensions of mass acceleration. The vector of pressures at all of the nodes $\mathbf{p}_{FE}$**,** which should not be confused with the vector of modal pressures along the cochlea in equation (1.8), is related to $\mathbf{q}_{FE}$ by the equation

$$\mathbf{Q}\ddot{\mathbf{p}}_{FE} + \mathbf{H}\mathbf{p}_{FE} = \mathbf{q}_{FE} \tag{5.1}$$

where **Q** is the mass matrix and **H** is the stiffness matrix in this case, as discussed, for example, by Fahy and Gardonio (2007). The imposed velocity at the BM has the half sinusoidal form shown in Fig. A1(b) and the discrete approximations to the modal velocity in equation (1.1) and modal pressure (1.2) are calculated from the relevant elements of $\mathbf{q}_{FE}$ and $\mathbf{p}_{FE}$ respectively. In fact, due to the symmetry of the assumed model, only the upper chamber needs to be modelled and the modal pressure difference is calculated as twice the modal pressure in this chamber.

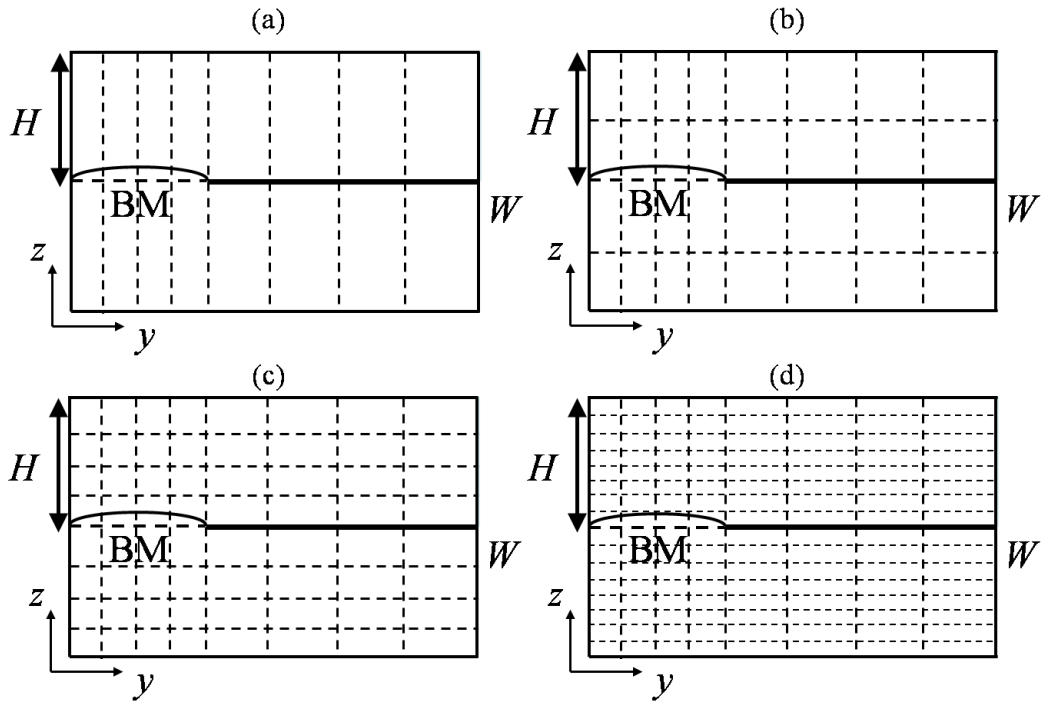

Fig. 5.1 *Grids used for finite element calculation of fluid coupling for a cross section of the cochlea. (a) 8 ×1 elements; (b) 8 × 2 elements; (c) 8 × 4 elements and (d) 8 × 8 elements.*

The rectangular box geometry was used in order to ensure compatibility with the analytic results above, and this was divided into 512 longitudinal sections for the same reason. The meshing in the cross section has to be finer than this in order to capture the near field pressure variation close to the vibrating BM, and four different mesh sizes were used to investigate the effect of this on the predicted result. Fig. 5.1 shows the geometry of the FE meshes used in these calculations for a cross section of the cochlea.

Fig. 5.2 shows the distribution along the cochlea of the computed modal pressure difference on the BM, when driven by a single longitudinal BM segment at different locations, for various mesh sizes in the FE model. It can be seen that with relatively few elements, the FE model reproduces the long wavelength behaviour of the pressure reasonably well, but a larger number of elements are required to reproduce the nearfield pressure on the BM and hence the additional short wavelength component of the modal pressure. The results with the smaller mesh size are in good agreement with those computed from the analytic model and shown in Fig. 2.6.

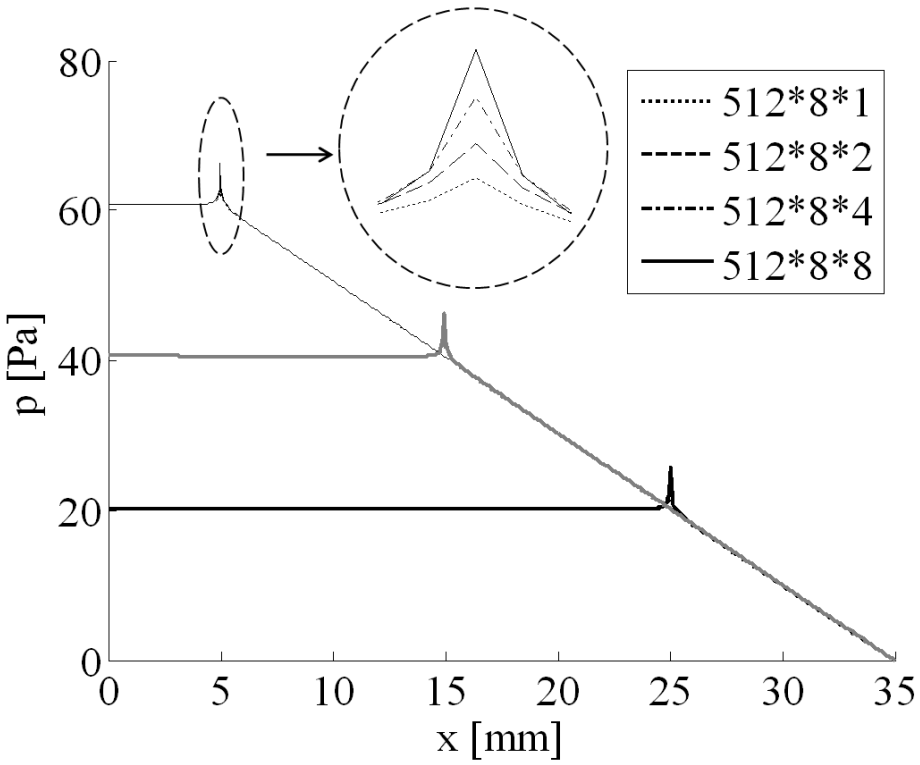

Fig. 5.2 *Modal pressure difference on the BM calculated using the FE model for excitation of a single longitudinal segment of the BM at x equal to 5 mm, 15 mm and 25 mm with a velocity of 10 mm·s^{-1} at a frequency of 1 kHz with* 8 ×1 elements (dotted), 8 × 2 elements (dashed), 8 × 4 elements (dot-dashed), 8 × 8 elements (sold).

An advantage of the finite element method is that since the fluid is modelled using acoustic elements, the compressibility of the fluid, as well as its inertial properties, are taken into account. The widely-used theoretical model described in the Appendix and used in Section 2 assumes that the fluid is incompressible. The effects of compressibility are expected to be greater at higher frequencies as the inertial forces become larger. Fig. 5.3 shows the magnitude of the modal pressure difference calculated using the finite element model, with the BM driven at equal accelerations on a single element at *x* equal to 5 mm, for excitation at 1 kHz, 10 kHz, 15 KHz and 20 kHz. In the incompressible model the fluid pressure would be independent of frequency. It is clear, however, that the magnitude and shape of the fluid pressure changes significantly with frequency in the finite element model. The magnitude increases at 10 kHz and the distribution of fluid pressure is no longer linear away from the excitation point.

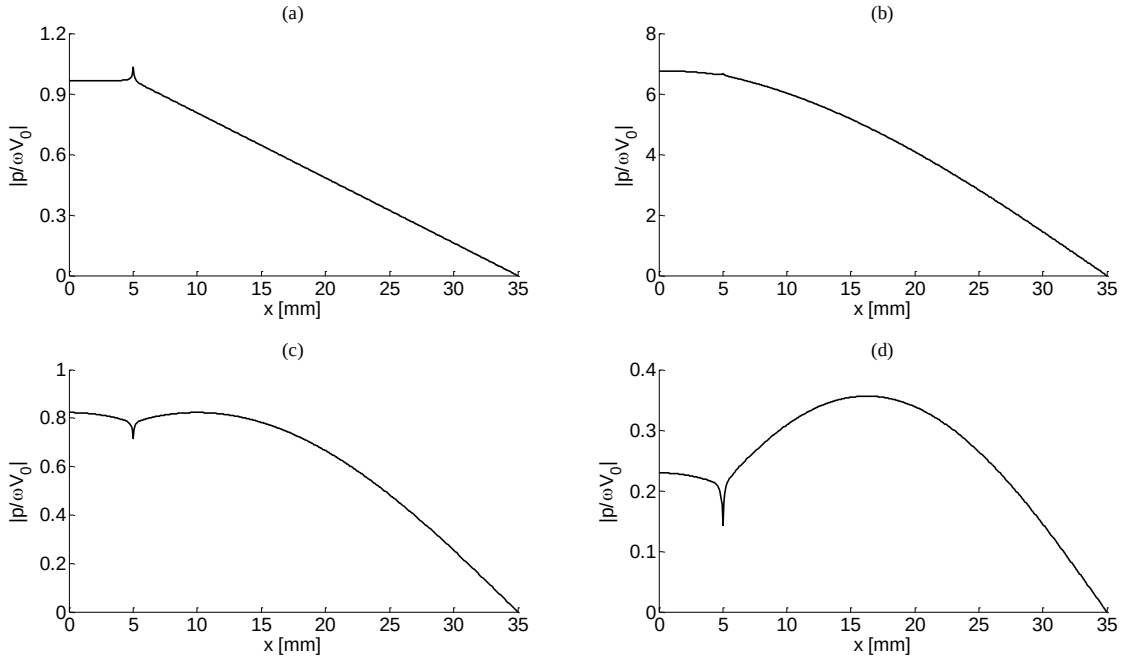

Fig. 5.3 *Magnitude of the modal pressure difference on the BM calculated using the finite element model for excitation of a single longitudinal element at x equal to 5 mm, normalised to the acceleration of the driving position at frequencies of (a) 1 kHz, (b) 10 kHz, (c) 15 kHz, (d) 20 kHz.*

Fig. 5.4 shows the predicted magnitude of the modal pressure at the base of the cochlea as a function of frequency. The peak at about 10.7 kHz can be associated with a resonance in the fluid column, which for the pressure difference has a rigid boundary condition where it is driven at the stapes and a pressure release boundary condition at the helicotrema. The cochlea length, 35 mm, thus corresponds to a quarter of a wavelength at this frequency, for an assumed wave speed of 1,500 ms^{-1}, which is the speed of a "fast wave" in the cochlea. This acoustic resonance increases the magnitude of the average pressure across any cross section of the cochlea, but does not influence the short-wavelength components which are unaffected by the compressibility of the fluid (Lighthill, 1981). In order to limit the pressure magnitude at this peak, the finite element model has been modified to include a small imaginary component in the elements of the **H** matrix in equation (5.1) so that each element is multiplied by $1 + i\eta$, where η is the loss factor. The loss factor was set equal to 0.03 for these simulations. The resonant peak at 10.7 kHz is accompanied by a phase change, so that the pressure distributions for excitation frequencies between 10.7 kHz and 20 kHz are almost entirely out of phase with those below 10.7 kHz.

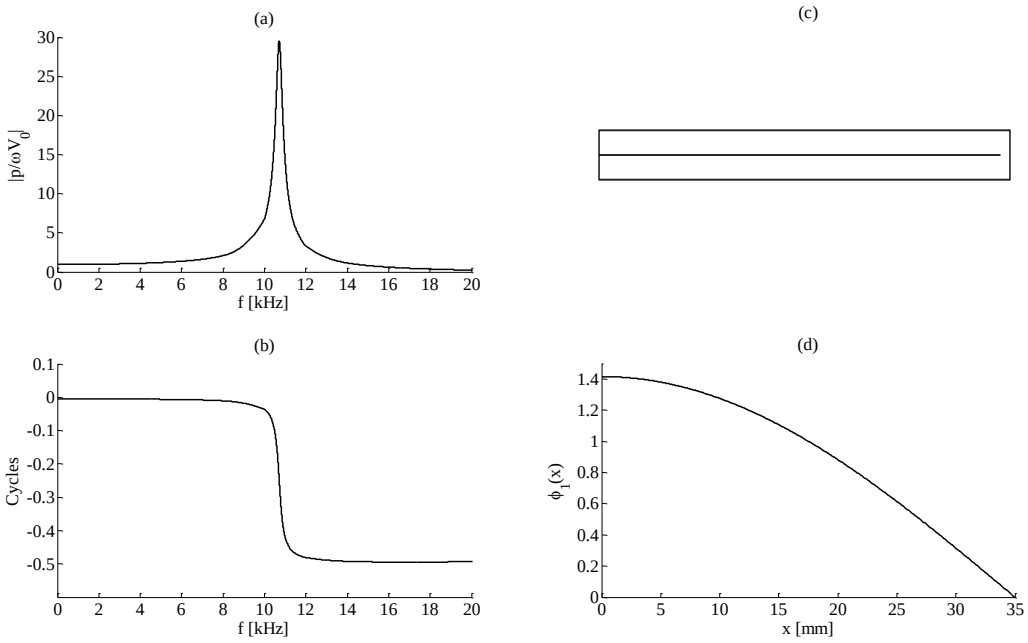

Fig. 5.4 *The magnitude (a) and phase (b) of the modal pressure difference at the base of the cochlea as a function of excitation frequency, calculated using the finite element method for excitation of a single longitudinal element at x equal to 5 mm. Also shown (c) is a sketch of the box model with the antisymmetric pressure driven by the BM velocity and the resulting pressure distribution when L is one quarter wavelength with the rigid boundary condition at the oval window and zero pressure difference at the helicotrema.*

It is interesting to compare the predicted frequency of this quarter wavelength resonance with the upper frequency of hearing in several species (Greenwood, 1990; Le Page, 2003), as in Table 5.1. This resonance appears to occur, perhaps coincidentally, at about half the upper frequency limit of hearing in each of these cases.

Table 5.1 *Cochlea length, upper frequency limit of hearing and calculated frequency of quarter wavelength resonance in fluid coupling for several species.*

Species	**Length of cochlea**	**Characteristic frequency at base**	**Frequency of $\lambda/4$ resonance**
Human	35 mm	21 kHz	10.7 kHz
Guinea Pig	18.5 mm	44 kHz	20.3 kHz
Gerbil	12.1 mm	63 kHz	31.0 kHz
Mouse	6.8 mm	105 kHz	55.1 kHz

Although this acoustic resonance is, in retrospect, simple to predict, its existence for the pressure difference component and its effect on cochlea mechanics does not appear to have previously been widely considered. Peterson and Bogert (1950) and Lighthill (1981) discuss a quarter wavelength resonance in the mean pressure component, but this is associated with a pressure source driving the cochlea as a closed duct, in order to match the pressure release boundary condition at the round window, and does not appear to be to the same as the quarter wavelength resonance in the pressure difference seen here.

If the cochlear fluid is assumed to be compressible (Peterson and Bogert, 1950), then the one-dimensional continuity equation (A30) becomes, in terms of the complex variables used here

$$\frac{\partial u(x)}{\partial x} + \frac{2i\omega}{\rho_0 {c_0}^2}\, p(x) = \frac{v(x)}{h}, \tag{5.3}$$

where $\rho_0 {c_0}^2$ is the bulk modulus of the fluid. Combining this with the equation for the conservation of momentum, (A31),

$$\frac{\partial p(x)}{\partial x} = -2i\omega\rho u(x), \tag{5.4}$$

gives a wave equation, which is the generalisation of the fluid coupling equation (2.4) for a compressible fluid, given by

$$\frac{\partial^2 p(x)}{\partial x^2} + \frac{\omega^2}{{c_0}^2}\, p(x) = -\frac{2i\omega\rho}{h} v(x). \tag{5.5}$$

The pressure is assumed to be uniform over the cochlear cross section in this analysis, giving a long wavelength solution, which in this case is the superposition of plane acoustic waves.

Assuming a zero pressure gradient at the stapes, a zero pressure difference at the helicotrema and continuity at x_0, where there is an assumed BM velocity of v_0 over a length Δ, then by assuming forward and backward travelling fast waves in the two regions of the cochlea the pressure difference can be shown to be

$$p(x) = \frac{i2\omega\rho}{k_0 h} \frac{\sin k_0 (L - x_0) \cos k_0 x}{\cos k_0 L} \Delta v_0 \quad \text{for} \quad 0 < x < x_0 - \Delta \tag{5.6}$$

and

$$p(x) = \frac{i2\omega\rho}{k_0 h} \frac{\cos k_0 x_0 \sin k_0 (L - x)}{\cos k_0 L} \Delta v_0 \quad \text{for } x_0 < x < L, \tag{5.7}$$

where k_0 is equal to ω / c_0 and c_0 is the compressional wave speed, assumed here to be 1,500 m·s^{-1}. Viscous losses can be taken into account in this case, where the viscous boundary layer is thin compared with the dimensions of the fluid duct, by defining a complex wavenumber with a real part still equal to ω / c_0 to a first approximation and an imaginary part of α, so that

$$k_0 = \frac{\omega}{c_0} - i\alpha. \tag{5.8}$$

An estimate of the attenuation coefficient, α, can be obtained by noting that it is proportional to the square root of the coefficient of viscosity, which is approximately 7×10^{-4} kg m^{-1}s^{-1} for cochlea fluids, compared with a value of 2×10^{-5} kg m^{-1}s^{-1} for air, and that for air in a circular duct, α is about $3 \times 10^{-5} \sqrt{f / a}$ where f is the frequency and a is the radius of the duct. Assuming that the equivalent cochlea duct has an area of W^2, then in this case

$$\alpha \approx 2\times 10^{-4}\sqrt{\frac{f}{W}}. \tag{5.9}$$

A complete analysis would involve the thermal as well as the viscous losses as described, for example, by Fletcher and Rossing (1998). These authors also discuss how numerical methods can be used to calculate the acoustic properties of a non-uniform duct by dividing it up into a large number of segments. The complex wavenumber in equation (5.8) can also be written as

$$k_0 = \frac{\omega}{c_0}(1 - i\eta/2), \tag{5.10}$$

where

$$\eta = \frac{2\alpha c_0}{\omega} \tag{5.11}$$

is the loss factor in the bulk modulus, assumed to be small compared with unity, that was used to introduce damping into the finite element model above. Although this loss factor clearly depends on frequency, the loss factor only significantly affects the response around resonance, so the frequency was set to 10 kHz in equation (5.11) to calculate the value of loss factor, 0.03, used in these simulations.

The effect of the fluid compressibility on the wavenumber of the slow cochlear wave is also predicted by the analysis of Peterson and Bogert (1950). Noting that their equation (14) denotes a dynamic stiffness, which in our notation can be written as $i\omega / \mathrm{Y}_{\mathrm{BM}}(i\omega)$, and setting their $s_0 b$ equal to h, equation (16) in Peterson and Bogert (1950) can be used to show that the modified wavenumber is equal to

$$k(x,\omega) = \sqrt{\frac{-2i\omega\rho}{h}\mathrm{Y}_{\mathrm{BM}}(x,\omega) + \frac{\omega^2}{{c_0}^2}}, \tag{5.12}$$

where c_0 is the speed of sound in the fluid. The wavenumber is thus not significantly affected by the compressibility since the maximum speed of the slow wave is about 70 m/s, which is much smaller than the 1,500 m/s speed of the fast wave.

Figure 5.5 compares the coupled BM velocity, calculated using the elemental approach outlined in Section 1, when the fluid coupling is assumed to be incompressible, as in Section 2, and compressible, as in this section. For simplicity, the short wavelength components have not been considered in either case here and the BM mass for the passive BM model has been set to include the additional fluid loading, as in Section 3. The columns of the fluid coupling impedance, $\mathbf{Z}_{FC}$, used in the solution to the coupled dynamics, equation (1.14), are obtained either from samples of the analytic form of the pressure for the incompressible case given by equations (2.23) and (2.24) or from samples of the analytical form of the pressure for the compressible case given by equations (5.6) and (5.7).

Despite the very significant change in the pressure distributions in the fluid coupling calculations due to fluid compressibility, as shown in Fig. 5.3, this hardly appears to have any effect on the coupled cochlea response at all. This surprising result can perhaps be understood by returning to the way in which the coupled model is formulated in Section 1. The fluid coupling effects are first calculated independently of any BM motion by defining the fluid coupling impedance matrix, equation (1.10), for the fluid chambers having rigid walls. It is this assumption that leads to the quarter wavelength resonance in the uncoupled fluid column. When the BM is allowed to move, in the coupled response, however, this resonance does not get a chance to become established since the BM is sufficiently mobile that it substantially equalises the pressures in the two fluid chambers well before the wave reaches the end of the cochlea.

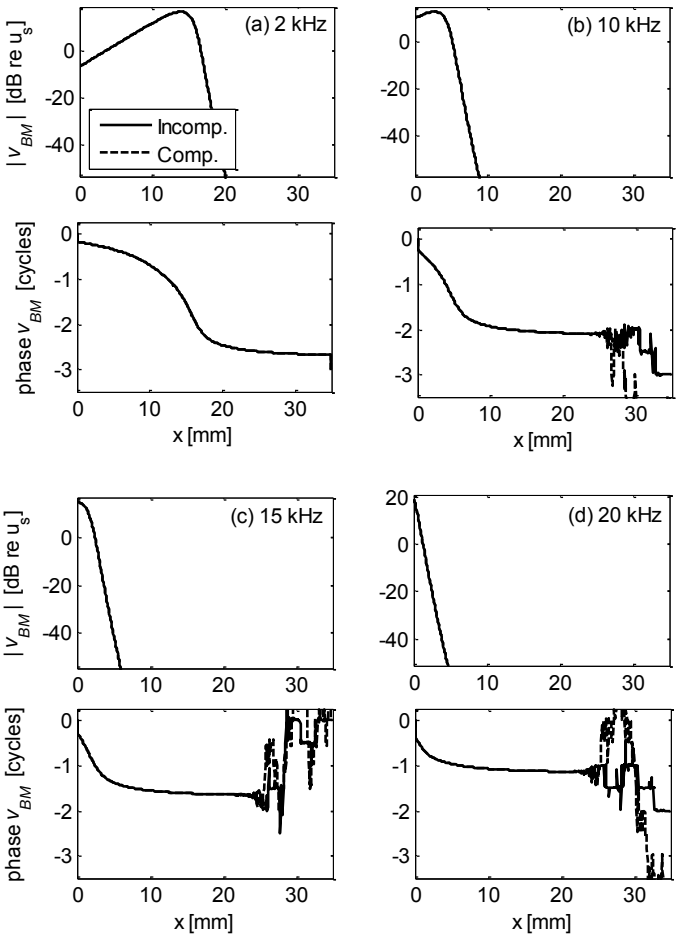

Fig. 5.5 *The coupled BM velocity calculated for high frequency excitation using the passive BM dynamics and long wavelength fluid coupling with the assumption that the fluid is either incompressible (solid lines) or compressible (dashed lines).*

6. State Space Representation

Both the short wavelength components of the fluid coupling and the effects of fluid compressibility can be accounted for by representing the pressure distribution as a modal series in a generalisation of the state space formulation for the coupled cochlear mechanics (Elliott *et al.*, 2007). The state space formulation can be used both to determine whether a linear model is or is not stable, and as the basis for time domain simulations of nonlinear models. In this report, the BM dynamics are assumed to be both passive and linear, so that stability is guaranteed and frequency domain methods are always valid. In the more general case of an active BM model, however, stability cannot be guaranteed and must be checked before the results of frequency domain calculations can be relied upon.

In this section the modal analysis of long wavelength coupling is first presented, since it is directly comparable to the plane wave analysis for a compressible fluid presented in the previous section. The more general case is then considered in which cross modes are also incorporated in the modal summation. This allows inclusion of the nearfield pressure close to the BM, and hence the short wavelength component of modal pressure difference, although the large number of acoustic modes required for convergence may not be the most efficient representation of these effects. Finally, the modal series representation for the fluid coupling is written in the time domain, which allows the derivation of a state space form for the fluid coupling. This can then be combined with a description of the BM dynamics to provide a state-space formulation for the coupled cochlear dynamics.

The complex pressure in an enclosure can be represented in terms of the sum of the contributions from a number of acoustic modes (Morse, 1948; Nelson and Elliott, 1992), so that the one-dimensional pressure distribution in one fluid chamber is given by

$$p_c(x,\omega) = \sum_{m=0}^{\infty} a_m(\omega)\phi_m(x), \tag{6.1}$$

where $a_m(\omega)$ is the complex modal amplitude and $\phi_m(x)$ is the one dimensional acoustic mode shape for a single fluid chamber. Although, in principle, the

summation should be taken over an infinite number of terms, very good approximations to the pressure distribution can be obtained in practice by using a finite number of terms.

The orthonormal mode shapes for the uniform box model that meet the boundary conditions for the pressure difference, so that there is zero pressure gradient at the stapes and zero pressure at the helicotrema, are

$$\phi_m(x) = \sqrt{2}\cos\frac{\pi(2m+1)x}{2L}. \tag{6.2}$$

The first mode, $m = 0$, corresponds to having a quarter wavelength along the cochlea, the second, $m = 1$, to three quarter wavelengths, etc. The corresponding natural frequencies for these modes are thus

$$\omega_m = \frac{\pi(2m+1)c_0}{2L}. \tag{6.3}$$

To calculate the pressure distribution due to a single element of the BM, we assume that the excitation is concentrated at the position x_0 and has a volume velocity of $q(x_0)$. The complex model amplitude can then be written as

$$a_m(\omega) = \frac{\omega\rho_0 {c_0}^2 \phi_m(x_0)\ q(x_0)}{V(2\zeta_m\omega_m\omega + i(\omega^2 - {\omega_m}^2))}, \tag{6.4}$$

where ζ_m is the modal damping ratio, V is the volume of the enclosure, which is equal to LWH, where H is the physical height of the fluid chamber. The volume velocity can be calculated by multiplying Δ by the integral of the radial velocity distribution over the BM width. The assumed radial velocity distribution is

$$v(y) = v_0\psi(y), \tag{6.5}$$

where v_0 is the modal velocity and $\psi(y)$ is the normalised velocity distribution given by equation (A21), with C equal to zero in this case. Integrating this distribution over the BM width gives the volume velocity at x_0 as

$$q(x_0) = \frac{2\Delta v_0}{\pi}\sqrt{2BW}. \tag{6.6}$$

Since the first natural frequency is about 10.7 kHz, the response below about 5 kHz can be estimated by taking the low frequency approximation for the mode amplitude, given by

$$\lim_{\omega << \omega_m} a_m(\omega) = \frac{i\omega\rho_0 {c_0}^2}{LWH\ {\omega_m}^2}\phi_m(x_0)q(x_0), \tag{6.7}$$

so that using equation (6.3) for ω_m,

$$\lim_{\omega << \omega_m} a_m(\omega) = \frac{4i\omega\rho_0 L}{\pi^2 WH(2m+1)^2}\phi_m(x_0)q(x_0). \tag{6.8}$$

The total pressure distribution in each chamber is then

$$\lim_{\omega << \omega_1} p_c(x) = \frac{4i\omega\rho_0 L q(x_0)}{\pi^2 WH}\sum_{m=0}^{\infty}\frac{\phi_m(x)\phi_m(x_0)}{(2m+1)^2}. \tag{6.9}$$

The modal pressure difference required here can be written as

$$p(x) = \frac{2}{W}\int p_c(x)\psi(y)dy = \frac{4p_c(x)}{\pi}\sqrt{\frac{2B}{W}}. \tag{6.10}$$

Using equation (6.6) for $q(x)$, and equation (6.2) for the mode shapes, the modal pressure difference at the base of the cochlea due to a source at the base, can be written in the low frequency limit as

$$\lim_{\omega << \omega_1} p(0) = \frac{128i\omega\rho_0 L\Delta v_0 B}{\pi^4 WH}\sum_{m=0}^{\infty}\frac{1}{(2m+1)^2}. \tag{6.11}$$

The infinite sum at the end of this equation is equal to $\pi^2/8$, allowing equation (6.11) to be written in the same form as the long wavelength pressure derived from the analysis above, assuming an incompressible fluid, in equation (2.23) as

$$p(0) = \frac{2i\omega\rho_0 L\Delta v_0}{h}, \tag{6.12}$$

where the effective height, h, can again be written as

$$h = \frac{\pi^2 WH}{8B}. \tag{6.13}$$

This modal analysis thus provides an independent check on the equation for the equivalent height from the wavenumber analysis in the Appendix.

The general form of the fluid pressure distribution in the upper chamber, incorporating the nearfield contributions can also be written as

$$p_c(x, y, z, \omega) = \sum_{m=0}^{\infty} a_m(\omega)\phi_m(x, y, z), \tag{6.14}$$

where m now denotes the trio of integers, m_1, m_2, and m_3 that characterise the modes in the x, y and z directions and in practice this infinite summation can again be truncated to arbitrary accuracy by a finite number of terms.

The orthonormal mode shapes of a rectangular enclosure that satisfy hard walled conditions on all sides of the fluid chamber, except for a pressure release condition at x equal to L are

$$\phi_m(x, y, z) = \sqrt{2\varepsilon_{m_2}\varepsilon_{m_3}} \cos\frac{(1+2m_1)\pi x}{2L} \cos\frac{m_2\pi y}{W} \cos\frac{m_3\pi z}{H}, \tag{6.15}$$

where ε_{m_2} and ε_{m_3} are normalisation constants equal to 1 if m_2 or m_3 equals zero and are otherwise equal to 2, with corresponding natural frequencies

$$\omega_m = c_0 \left[\left(\frac{(1+2m_1)\pi}{2L} \right)^2 + \left(\frac{m_2\pi}{W} \right)^2 + \left(\frac{m_3\pi}{H} \right)^2 \right]. \tag{6.16}$$

Interestingly, Neely (1985) uses a similar modal expansion for the pressure in his derivation of the three dimensional fluid coupling, although he assumes a zero velocity boundary condition at the apical end of the cochlea rather than the pressure release one here.

The modal amplitudes in this case, when excited by a BM element of length Δ, which is assumed to be small compared with L, and radial velocity equal to $v_{n'}\psi(y)$ at position $x_{n'}$ is equal to

$$a_m(\omega) = \frac{\omega\rho_0 {c_0}^2 \Delta v_{n'}}{V(2\zeta_m\omega_m\omega + i(\omega^2 - {\omega_m}^2))} \int_0^W \phi_m(x_{n'}, y, 0)\psi(y)dy, \tag{6.17}$$

where for half sinusoidal radial velocity distributions the integrals are similar to those evaluated in equations (A22) and (A23).

The modal pressure difference at position x_n, again assuming Δ is small compared with L, is then

$$p(x_n) = \sum_{m=0}^{\infty} a_m(\omega)\frac{2}{W}\int_0^W \phi_m(x_n, y, 0)\psi(y)dy. \tag{6.18}$$

The modal pressure at the n-th BM element, including near field components, can thus be calculated due to the modal motion of the n-th BM element, as required for the discrete model.

This set of frequency domain expressions for the modal pressure can also be expressed in matrix form. The vector of complex modal pressures, $\left[p_1, p_2, \cdots p_N\right]^{\mathrm{T}}$, can be written as

$$\mathbf{p}(\omega) = \mathbf{\Phi}\mathbf{a}(\omega), \tag{6.19}$$

where the m, n-th element of $\mathbf{\Phi}$ corresponds to the integral in equation (6.18) and $\mathbf{a}(\omega)$ is the vector of M modal amplitudes. These complex modal amplitudes can also be written as

$$\mathbf{a}(\omega) = \mathbf{B}\mathbf{\Phi}^{\mathrm{T}}\mathbf{v}(\omega), \tag{6.20}$$

where $\mathbf{B}$ is a diagonal matrix whose m-th element can be deduced from equation (6.17) and $\mathbf{v}(\omega)$ is the vector of N velocities, including the first element equal to the

normalised stapes velocity, the $N-2$ BM velocities and the N-th element equal to zero at the helicotrema.

The vector of complex modal pressures can thus be written in terms of the complex driving velocities as

$$\mathbf{p} = \mathbf{\Phi B \Phi}^{\mathrm{T}} \mathbf{v}, \tag{6.21}$$

where $\mathbf{\Phi B \Phi}^{\mathrm{T}}$ constitutes the matrix of fluid coupling impedances $\mathbf{Z}_{\mathrm{FC}}$ in this case.

The general form of the modal series for the fluid coupling can now be put into state space form by assuming that only a finite number of modes are considered. In the continuous spatial domain, the modal pressure difference as a function of frequency is

$$p(x,\omega) = \sum_{m=0}^{M} a_m(\omega)\phi_m(x). \tag{6.22}$$

where $\phi_m(x)$ is either the one dimensional mode shape or the result of the integral over the three dimensional mode shape shown in equation (6.18).

If the fluid chambers are excited by a modal BM velocity of $v_{n'}(\omega)$ at a position $x_{n'}$, the modal amplitude is

$$a_m(\omega) = \frac{A_{mn'}\omega v_{n'}(\omega)}{2\zeta_m\,\omega_m\omega + i(\omega^2 - {\omega_m}^2)}, \tag{6.23}$$

where

$$A_{mn'} = \frac{16\rho_0 {c_0}^2 B\Delta}{\pi^2 \nu} \int_0^W \phi_m(x_{n'}, y, 0)\psi(y)dy. \tag{6.24}$$

The expression for the complex mode amplitude may be written as

$$\omega_m^2 a_m(\omega) + 2i\zeta_m\omega_m\omega a_m(\omega) - \omega^2 a_m(\omega) = i\omega A_{mn'}v_{n'}(\omega). \tag{6.25}$$

With a slight abuse of notation, this expression for the modal amplitude in the frequency domain can be written in time domain form as

$$\omega_m^2 a_m(t) + 2\zeta_m \omega_m \dot{a}_m(t) + \ddot{a}_m(t) = A_{mn'} \dot{v}_{n'}(t). \tag{6.26}$$

This may be written in state space form as

$$\begin{bmatrix} \ddot{a}_m(t) \\ \dot{a}_m(t) \end{bmatrix} = \begin{bmatrix} -2\zeta_m \omega_m & -\omega_m{}^2 \\ 1 & 0 \end{bmatrix} \begin{bmatrix} \dot{a}_m(t) \\ a_m(t) \end{bmatrix} + \begin{bmatrix} A_{mn'} \\ 0 \end{bmatrix} \dot{v}_{n'}(t). \tag{6.27}$$

The complete state vector for the fluid modes can be written as

$$\mathbf{x}_F(t) = \left[\dot{a}_0(t)\ a_0(t)\ \dot{a}_1(t)\ a_1(t) \ldots \dot{a}_M(t)\ a_M(t) \right]^{\mathrm{T}}, \tag{6.28}$$

so that the dynamics of all the fluid modes can be expressed as

$$\dot{\mathbf{x}}_F(t) = \mathbf{A}_F \mathbf{x}_F(t) + \mathbf{B}_F \dot{\mathbf{v}}(t), \tag{6.29}$$

where $\mathbf{A}_F$ has diagonal blocks for each pair of modal states, as above, $\mathbf{B}_F$ has elements $A_{mn'}$ or zero and $\mathbf{v}(t)$ is the vector of velocities along the BM,

$$\mathbf{v}(t) = \left[v_2(t), v_3(t), \cdots v_{N-1}(t) \right]^{\mathrm{T}}, \tag{6.30}$$

where as above, the BM extends from the 2nd to (N – 1)-th element to account for the stapes and helicotrema dynamics at the 1st and N-th element, respectively.

The complex pressure difference at the n-th location along the cochlea can thus be written, assuming Δ is very small compared with L, as

$$p_n(\omega) = \sum_{m=0}^{M} a_m(\omega) \phi_m(x_n), \tag{6.31}$$

where $\phi_m(x_n)$ has the same generalised meaning as above. In the time domain the pressure difference at this location is, again with a slight abuse of notation,

$$p_n(t) = \sum_{m=0}^{M} a_m(t)\phi_m(x_n). \tag{6.32}$$

The vector of pressure time histories at the N locations along the cochlea can thus be written as

$$\mathbf{p}(t) = \mathbf{C}_F \mathbf{x}_F(t), \tag{6.33}$$

where $\mathbf{C}_F$ contains elements $\phi_m(x_n)$ that pick out the corresponding modal amplitudes.

The dynamics of the BM elements can also be represented in a general state space form (Elliott *et al*., 2007) and written as

$$\dot{\mathbf{x}}_E(t) = \mathbf{A}_E \mathbf{x}_E(t) + \mathbf{B}_E \mathbf{p}(t), \tag{6.34}$$

where $\mathbf{x}_E(t)$ is the vector of state variables associated with the displacements and velocities of all the masses involved in the BM dynamics, and $\mathbf{A}_E$ and $\mathbf{B}_E$ contain the mechanical parameters of the BM dynamics and also those of the middle ear and helicotrema. The BM velocities driving the fluid can also be written as

$$\mathbf{v}(t) = \mathbf{C}_E \mathbf{x}_E(t), \tag{6.35}$$

where $\mathbf{C}_E$ picks out the relevant elements of $\mathbf{x}_E(t)$. The BM accelerations are thus

$$\dot{\mathbf{v}}(t) = \mathbf{C}_E \dot{\mathbf{x}}_E(t), \tag{6.36}$$

where $\dot{\mathbf{x}}_E(t)$ is given by the state space model of the BM elements above, equation (6.34), so that

$$\dot{\mathbf{v}}(t) = \mathbf{C}_E \mathbf{A}_E \mathbf{x}_E(t) + \mathbf{C}_E \mathbf{B}_E \mathbf{C}_F \mathbf{x}_F(t), \tag{6.37}$$

where the expression for $\mathbf{p}(t)$ in terms of the fluid state variables, equation (6.33), has also been used.

The dynamics of the fluid states, equation (6.29), can thus be written as

$$\dot{\mathbf{x}}_F(t) = \left[\mathbf{A}_F + \mathbf{B}_F\mathbf{C}_E\mathbf{B}_E\mathbf{C}_F\right]\mathbf{x}_F(t) + \mathbf{B}_F\mathbf{C}_E\mathbf{A}_E\mathbf{x}_E(t). \tag{6.38}$$

If the vector containing both the fluid and BM dynamics states is defined as

$$\mathbf{x} = \begin{bmatrix} \mathbf{x}_E \\ \mathbf{x}_F \end{bmatrix}, \tag{6.39}$$

the coupled behaviour of the cochlea can be described by the overall state space equations

$$\mathbf{x} = \mathbf{A}\mathbf{x} + \mathbf{B}\mathbf{p}, \qquad \mathbf{v} = \mathbf{C}\mathbf{x}, \tag{6.40}$$

where

$$\mathbf{A} = \begin{bmatrix} \mathbf{A}_E & \mathbf{0} \\ \mathbf{B}_F\mathbf{C}_E\mathbf{A}_E & \mathbf{A}_F + \mathbf{B}_F\mathbf{C}_E\mathbf{B}_E\mathbf{C}_F \end{bmatrix}, \tag{6.41}$$

$$\mathbf{B} = \begin{bmatrix} \mathbf{B}_E \\ \mathbf{0} \end{bmatrix}, \qquad \mathbf{C} = \begin{bmatrix} \mathbf{C}_E \\ \mathbf{0} \end{bmatrix}. \tag{6.42, 6.43}$$

7. Incorporation of short wavelength fluid coupling into a modified BM admittance

One disadvantage of incorporating short wavelength fluid coupling into the fluid coupling impedance of a discrete model is that the inverse of this impedance is no longer tri-diagonal, as it is in the case of long wavelength fluid coupling in equation (2.18) above. There can be significant numerical advantages to retaining this tri-diagonal form for the inverse of the fluid coupling matrix, in both a frequency domain (Neely, 1981) and a time domain (Moleti *et al.*, 2009) formulation. In this section we demonstrate how the short wavelength fluid coupling can be incorporated into a modified form of the BM admittance matrix.

We initially return to the matrix form of the solution for the vector of modal pressure differences along the length of the cochlea, derived in the introduction, where, at a single frequency,

$$\mathbf{p} = \mathbf{p}_s + \mathbf{Z}_{FC}\mathbf{v} \quad \text{and} \quad \mathbf{v} = -\mathbf{Y}_{BM}\mathbf{p}, \tag{7.1, 7.2}$$

so that

$$\mathbf{p} = \left[\mathbf{I} + \mathbf{Z}_{FC}\mathbf{Y}_{BM}\right]^{-1}\mathbf{p}_s, \tag{7.3}$$

where $\mathbf{Z}_{FC}$ is the total fluid coupling matrix, $\mathbf{Y}_{BM}$ is the matrix of BM admittances, which is diagonal if the BM is assumed to be locally reacting, and $\mathbf{p}_s$ is the vector of modal pressure differences due to the motion of the stapes in the cochlea, with a rigid BM, which is written as $\mathbf{z}_s u_s$ in equation (1.12) above. The first column of $\mathbf{Z}_{FC}$ is zero, since the contribution of the stapes velocity to the pressure is accounted for by $\mathbf{p}_s$. and the final column of $\mathbf{Z}_{FC}$ is also zero due to the pressure release boundary condition at the helicotrema. Although the first and last diagonal terms of $\mathbf{Y}_{BM}$ were set to zero above, we note that they can take arbitrary values and not affect the product $\mathbf{Z}_{FC}\mathbf{Y}_{BM}$ because the first and last columns of $\mathbf{Z}_{FC}$ are zero. Suitable small values are assumed to be inserted here to ensure that the $\mathbf{Y}_{BM}$ matrix can be inverted.

The vector of pressures is now divided up into long and short wavelength components so that

$$\mathbf{p} = \mathbf{p}_L + \mathbf{p}_{S,} \tag{7.4}$$

where $\mathbf{p}_L = \mathbf{p}_{Ls} + \mathbf{Z}_L\mathbf{v}$, (7.5)

and $\mathbf{p}_S = \mathbf{p}_{Ss} + \mathbf{Z}_S\mathbf{v}$, (7.6)

so that $\mathbf{p}_{Ls}$ and $\mathbf{p}_{Ss}$ are the long wavelength and short wavelength components of the pressure difference due to the stapes motion and $\mathbf{Z}_L$ and $\mathbf{Z}_S$ are the corresponding components of $\mathbf{Z}_{FC}$, as defined in Section 2.

The long wavelength component of the pressure thus satisfies the differential equation (2.4) and plays a similar role to the average pressure used by Shera *et al* (2005) in another transformation of general fluid coupling into an equivalent one-dimensional form.

We now explore the assumption that the BM velocity, $\mathbf{v}$, is generated only by the vector of long wavelength components of the pressure via a modified BM admittance, $\mathbf{Y}'_{BM}$, so that

$$\mathbf{v} = -\mathbf{Y}'_{BM}\mathbf{p}_L. \tag{7.7}$$

Combining this with the equation above for $\mathbf{p}_L$, gives

$$\mathbf{p}_L = \left[\mathbf{I} + \mathbf{Z}_L\mathbf{Y}'_{BM}\right]^{-1}\mathbf{p}_{Ls}. \tag{7.8}$$

In order for this equation to have more than just a formal significance, however, we need to put some physical interpretation on the modified BM admittance, $\mathbf{Y}'_{BM}$. This can be achieved if it assumed that the stapes motion does not generate a substantial component of short wavelength pressure, so that $\mathbf{p}_{Ss}$ in equation (7.6) is much less than that generated by the BM motion, $\mathbf{Z}_S\mathbf{v}$, in which case the short wavelength pressure is given by

$$\mathbf{p}_S = \mathbf{Z}_S\mathbf{v}. \tag{7.9}$$

This assumption may be less valid at very high frequencies when the moving part of the BM is close to the stapes, but seems reasonable at most frequencies. The

expressions for the velocity in terms of the total and long wavelength pressures in equations (7.2) and (7.7) above can also be written as

$$\mathbf{p} = -\mathbf{Z}_{\mathrm{BM}}\mathbf{v} \text{ and } \mathbf{p}_{\mathrm{L}} = -\mathbf{Z}'_{\mathrm{BM}}\mathbf{v}, \tag{7.10, 7.11}$$

where $\mathbf{Z}_{\mathrm{BM}}$ is the inverse of $\mathbf{Y}_{\mathrm{BM}}$ and $\mathbf{Z}'_{\mathrm{BM}}$ is the inverse of $\mathbf{Y}'_{\mathrm{BM}}$, assuming it is not singular. This allows the expression for the total pressure in terms of the long- and short wavelength components, equation (7.4), to be written as

$$-\mathbf{Z}_{\mathrm{BM}}\mathbf{v} = -\mathbf{Z}'_{\mathrm{BM}}\mathbf{v} + \mathbf{Z}_{\mathrm{S}}\mathbf{v}, \tag{7.12}$$

so that provided $\mathbf{v}$ is not zero,

$$\mathbf{Z}'_{\mathrm{BM}} = \mathbf{Z}_{\mathrm{BM}} + \mathbf{Z}_{\mathrm{S}}. \tag{7.13}$$

The modified BM admittance, $\mathbf{Y}'_{\mathrm{BM}}$, which is the inverse of this, thus incorporates the BM dynamics and the short wavelength components of the fluid coupling.

In general, however, $\mathbf{Z}_S$ will not be diagonal and so this matrix will introduce longitudinal coupling into the modified BM dynamics. It must be noted, however, that the locally-reacting assumption that originally led to the diagonal form of $\mathbf{Z}_{\mathrm{BM}}$ is only a first approximation to the true dynamics of the BM, and so the short wavelength mass coupling can be added to a list of other sources of longitudinal coupling that perhaps should be included in a complete model. These include BM damping (Mammano and Nobili 1993), TM elasticity (Zwislocki and Kletsky, 1979 ; Aranyosi *et al*., 2008), longitudinal electrical coupling (Parthasarathi *et al.*, 2000, for example), all of which have recently been compared by Meaud and Grosh (2010) and the feedforward action of the outer hair cells (Steele *et al.*, 1993; de Boer 1996).

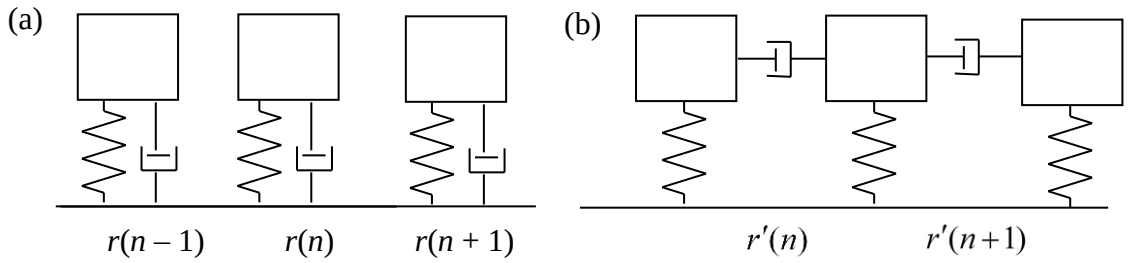

Fig. 7.1 *Array of 3 elements of the passive BM when damping is assumed to be locally-reacting (a), and when relative damping is assumed (b).*

The incorporation of relative BM damping into the BM impedance matrix can be used to illustrate how the BM impedance matrix can become non-diagonal if the BM dynamics are not locally reacting. Fig. 7.1(a) shows an array of 3 locally acting elements of a passive model of the BM, for which

$$\mathbf{Z}_{\mathrm{BM}} = \begin{bmatrix} 0 & 0 & 0 & & & \\ 0 & Z_{\mathrm{BM}}(2) & 0 & & & \\ & 0 & Z_{\mathrm{BM}}(3) & 0 & & \\ & & \ddots & & & \\ & & & 0 & Z_{\mathrm{BM}}(N-1) & 0 \\ & & & 0 & 0 & 0 \end{bmatrix}, \tag{7.14}$$

where

$$Z_{\mathrm{BM}}(n) = s(n)/i\omega + r(n) + i\omega m(n) \tag{7.15}$$

and $m(n)$, $s(n)$ and $r(n)$ are the mass stiffness and damping of the n-th BM element, so that $\mathbf{Z}_{\mathrm{BM}}$ is diagonal.

If damping in the BM is assumed to be primarily generated by relative motion of the individual elements, as suggested by Mammano and Nobili (1993), then the discrete elements take the form shown in Fig. 7.1(b). The pressure on the n-th element can now be written as

$$p(n) = -\{[s(n)/i\omega + i\omega m(n)]v(n) + [r'(n)(v(n) - v(n-1)) - r'(n+1)(v(n+1) - v(n))]\} \quad , \tag{7.16}$$

so that

$$p(n) = -\{Z'_{\mathrm{BM}}(n)v(n) - r'(n)v(n-1) - r'(n+1)v(n+1)\}, \tag{7.17}$$

where

$$Z'_{\mathrm{BM}}(n) = s(n)/i\omega + (r'(n) + r'(n+1)) + i\omega m(n). \tag{7.18}$$

and $r'(n)$ is the value of the relative damper.

The matrix of BM impedances now takes the form

$$\mathbf{Z}_{\mathrm{BM}} = \begin{bmatrix} 0 & 0 & 0 & & & & \\ -r'(2) & Z'_{\mathrm{BM}}(2) & -r'(3) & & & & \\ 0 & -r'(3) & Z'_{\mathrm{BM}}(3) & -r'(4) & & & \\ & & & \ddots & & & \\ & & & & -r'(N-1) & Z'_{\mathrm{BM}}(N-1) & -r'(N) \\ & & & & 0 & 0 & 0 \end{bmatrix}. \tag{7.19}$$

The effect of relative damping on the coupled BM response is illustrated in Fig. 7.2, in which the value of the relative damping has been adjusted to give the same peak response as that for the local damping. The numerical value of $r'(n)$ when used for relative damping is about four times that for local damping, $r(n)$, to achieve this condition in these simulations, even though, it is acknowledged that the units of $r(n)$ and $r'(n)$ are not same. The velocity responses with local and relative damping are surprisingly similar, apart from the more abrupt phase behaviour just beyond cut-off in the latter case, which can cause numerical problems if the damping is very light and an insufficient number of elements is used in the simulations. The pressure responses have similar phase behaviour and also show a small magnitude difference at the characteristic place.

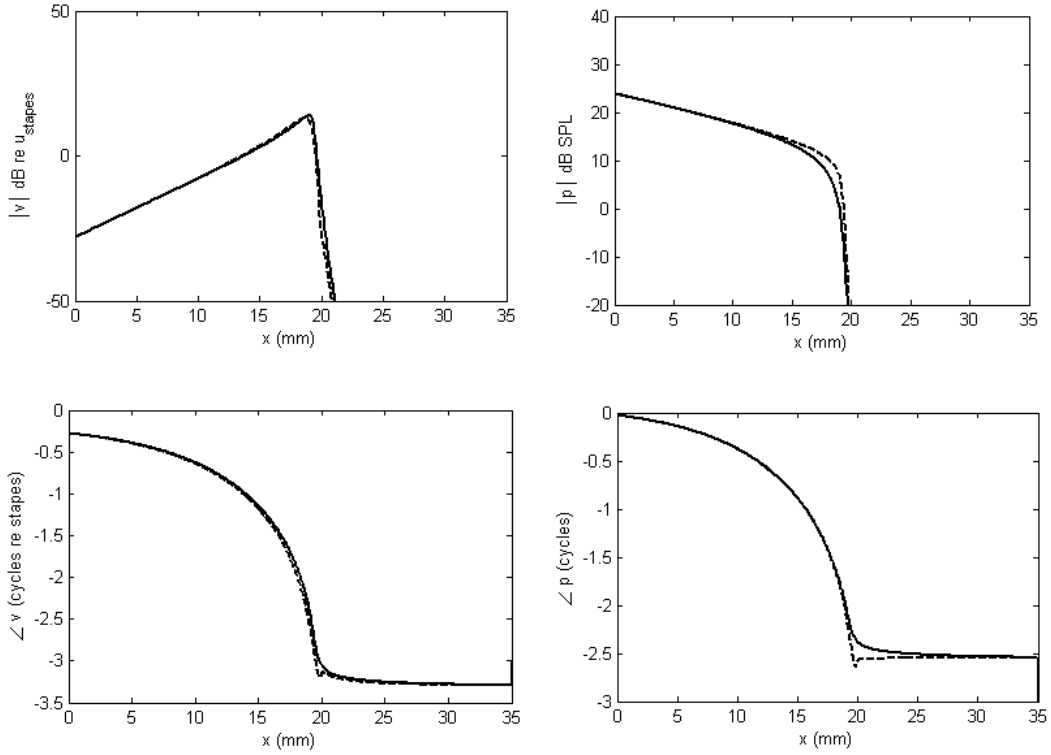

Fig. 7.2 *The BM velocity in the passive cochlea when damping is assumed to depend on the absolute motion of the BM elements, solid, and the relative motion of the BM elements, dashed, where the value of the damping has been adjusted in the former case to match the peak response of the latter.*

If the fluid coupling is approximated by a long wavelength term and a constant added mass, as discussed at the end of the Appendix, the modification of the BM impedance by an "added mass" is well known (de Boer, 1982; Neely, 1985). This modification of the assumed BM impedance would not affect the diagonal properties of $\mathbf{Z}_{BM}$. The analysis above has demonstrated how a complete description of short wavelength fluid coupling can be incorporated into a modified BM impedance matrix, thus generalising the "added mass" idea. The fact that $\mathbf{Z}_{BM}$ is then no longer diagonal reflects the fact that short wave fluid coupling gives rise to relatively local longitudinal coupling along the BM, in a similar way to relative damping. Although the effective BM impedance matrix is no longer diagonal, it is fairly tightly banded and so not too many terms need to be considered for an accurate solution in either the frequency or the time domains. These additional terms may not add significantly to the computational time, compared with the computational savings obtained by retaining a tridiagonal fluid coupling matrix, which can then be efficiently inverted.

8. Conclusions

An important simplification of the analysis between the fluid coupling and BM motion in cochlear mechanics can be obtained by defining a single longitudinal variable for the pressure difference and for the BM velocity. This reduces the three-dimensional fluid coupling problem down to a uniaxial one. If the coupling analysis is then performed in the continuous spatial domain, however, using the Green's function approach for example, singularities appear in the representation of the short wavelength fluid coupling due to the implicit assumption of a spatial delta function for the driving velocity.

By dividing up the uniaxial formulation into a discrete number of longitudinal sections, the problem becomes more tractable numerically, since it can be described using linear algebra. The singularity in the short wavelength fluid coupling term also disappears since the assumed BM velocity distributions remain finite. Realistic longitudinal variations in the geometry, including asymmetric fluid chambers, can also be readily incorporated. The short wavelength fluid coupling terms could then be readily incorporated into the fluid coupling matrix. Several authors have emphasised the numerical advantages of having a tridiagonal inverse of the fluid coupling matrix in order to obtain a solution in the frequency or time domain, however, which would imply that only long wavelength fluid coupling was included. It is shown that provided the stapes motion does not significantly contribute to the short wavelength pressure distribution, the matrix formulation with the full fluid coupling matrix can be recast into an equivalent formulation with only long wavelength fluid coupling. The effects of the short wavelength fluid coupling are then incorporated into a modified matrix of BM admittances, which is no longer diagonal even if the BM dynamics are locally reacting. Short wavelength fluid coupling then forms an additional longitudinal mass coupling term on the BM, together with distributed stiffness and damping.

In summary, three-dimensional fluid motion can be fully incorporated into the uniaxial formulation obtained from a simple box 1D model of the cochlea provided:

(1) Careful definitions of the 'modal' BM velocity and pressure difference are used.

(2) An effective height of the box model is used in the long wavelength coupling, which is greater than the physical height.

(3) The short wavelength effects of the fluid coupling are incorporated, with any other longitudinal coupling effects, as a modified BM admittance.

A modal model of the fluid coupling allows a generalisation of a previous state space description on the cochlear mechanics. A finite element model of fluid coupling is also used to provide an independent check of the results of the analytic model. The agreement between the incompressible analytic model and the finite element model is good for excitation frequencies below about 5 kHz, but the finite element model then predicts a more complicated pressure distribution, whose magnitude has a resonance at about 11 kHz. This is due to the fact that, unlike the analytic model, the finite element model takes into account the compressibility of the fluid, which thus has a finite speed of sound. The peak in the pressure difference response is associated with a quarter wavelength resonance in the cochlea, which is rigidly terminated at the oval window but has a pressure release boundary condition at the helicotrema. This resonance in the fluid coupling does not appear to significantly affect the coupled cochlear response, however, since the BM dynamics are then strongly coupled with the fluid dynamics and the rigid walled resonance does not become established.

Appendix: Wavenumber formulation for fluid coupling in the symmetric cochlea

In this Appendix the pressure difference across the BM is calculated, following Steele and Taber (1979), in the wavenumber domain for the box model of the cochlea, assuming it is symmetric, i.e., the two fluid chambers above and below the BM are of equal area. The pressure distributions in the two chambers are thus equal and opposite and it is convenient to work with the single distribution $p(x, y, z)$, equal to the pressure difference, which is twice the pressure in the upper chamber. The fluid is assumed to be incompressible and inviscid and so the conservation of fluid mass then leads to the equation

$$\frac{\partial^2 p(x,y,z)}{\partial x^2} + \frac{\partial^2 p(x,y,z)}{\partial y^2} + \frac{\partial^2 p(x,y,z)}{\partial z^2} = 0. \tag{A1}$$

The fluid chamber has a width of W and height H. Hard boundary conditions are assumed on the sides and the top of the cochlear channel above the BM, so that we must have

$$\frac{\partial p(x,y,z)}{\partial y} = 0 \quad \text{at } y = 0 \text{ and } W \tag{A2}$$

and

$$\frac{\partial p(x,y,z)}{\partial z} = 0 \quad \text{at } z = H. \tag{A3}$$

The fluid velocity at $z = 0$ must match that of the BM, so that

$$\frac{\partial p(x,y,z)}{\partial z} = -2i\omega\rho v_{\mathrm{BM}}(x,y) \qquad \text{at } z = 0, \tag{A4}$$

where the factor of 2 is due to the pressure doubling when $p(x, y, z)$ is defined as the pressure difference. The BM velocity is now assumed to have a given distribution across its width, and in the longitudinal direction it has a sinusoidal variation with wavenumber k, so that

$$v_{\mathrm{BM}}(x,y) = v(x)\psi(y) = V(k)\psi(y)e^{-ikx}, \tag{A5}$$

where $v(x)$ is the "modal" BM velocity distribution along the cochlea and $\psi(y)$ is the BM velocity distribution in the transverse direction. The velocity distribution $\psi(y)$ is normalised such that

$$\int_0^W \psi^2(y)dy = W, \tag{A6}$$

so that $v(x)$ can be calculated from $v_{\mathrm{BM}}(x, y)$ as

$$v(x) = \frac{1}{W}\int_0^W v_{\mathrm{BM}}(x,y)\psi(y)dy. \tag{A7}$$

The pressure field is assumed to be described by a summation of modes of the form

$$p(x,y,z) = \sum_{n=0}^{\infty} B_n\phi_n(y,z)e^{-ikx}, \tag{A8}$$

where each mode shape, $\phi_n(y,z)$, must satisfy the boundary conditions above. A suitable choice of pressure mode shape (Steel and Taber, 1979; Neely, 1985) is

$$\phi_n(y,z) = \cos\left(\frac{n\pi y}{W}\right)\cosh(m_n(z-H)). \tag{A9}$$

In order for each term in the model expansion to satisfy the equation for mass conservation, equation (A1), then the real parameter m_n must satisfy the equation

$$m_n^2 = k^2 + \frac{n^2\pi^2}{W^2}. \tag{A10}$$

The coefficients B_n are determined by the boundary condition at the BM, so that using equation (A4) with (A5) and (A8) gives

$$\sum_{n=0}^{\infty} B_n \frac{\partial\phi_n(y,z)}{\partial z} = -2i\omega\rho V(k)\psi(y) \quad \text{at } z = 0. \tag{A11}$$

If $\phi_n(y,z)$ is given by (A9), then equation (A11) can be written as

$$\sum_{n=0}^{\infty} B_n m_n \sinh(m_n H)\cos\left(\frac{n\pi y}{W}\right) = 2i\omega\rho\psi(y)V(k). \tag{A12}$$

Multiplying each side of (A12) by $\cos\left(n\pi y/W\right)$ and integrating from 0 to W over y, the orthogonality of the $\cos(n\pi y/W)$ function yields

$$B_n = \frac{2i\omega\rho A_n}{m_n \sinh(m_n H)} V(k), \tag{A13}$$

where the coupling coefficient for $n = 0$ is defined as

$$A_0 = \frac{1}{W}\int_0^W \psi(y)\,dy. \tag{A14}$$

and for n $\geq$ 1 is

$$A_n = \frac{2}{W}\int_0^W \cos\left(\frac{n\pi y}{W}\right)\psi(y)\,dy. \tag{A15}$$

We now explicitly define the "modal" pressure difference to be

$$p(x) = \frac{1}{W}\int_0^W p(x,y,0)\psi(y)dy. \tag{A16}$$

The longitudinal pressure distribution is defined to have this modal form so that the ratio of pressure to BM velocity is equal to the BM impedance, and the product of modal pressure and BM velocity is equal to acoustic power. The modal pressure can be written using (A8) and (A9) as

$$p(x) = \frac{1}{W}\sum_{n=0}^{\infty} B_n \cosh(m_n H)\int_0^W \cos\left(\frac{n\pi y}{W}\right)\psi(y)\,dy\,e^{-ikx}, \tag{A17}$$

so that using equations (A13), (A14) and (A15) and writing the modal pressure by analogy with the modal velocity in equation (A5) as

$$p(x) = P(k)e^{-ikx}, \tag{A18}$$

then

$$P(k) = i2\omega\rho\left[\frac{A_0^2}{k}\coth(kH) + \sum_{n=1}^{\infty}\frac{A_n^2}{2m_n}\coth(m_nH)\right]V(k), \tag{A19}$$

where the equation in brackets is equal to $Q(k)$ for the symmetric cochlea, which is thus equal to

$$\mathrm{Q}(k) = \frac{A_0^2}{k}\coth(kH) + \sum_{n=1}^{\infty}\frac{A_n^2}{2m_n}\coth(m_nH). \tag{A20}$$

To proceed further, the form of the BM vibration across the cochlea has to be assumed, to define $\psi(y)$ in equation (10). We assume here that BM takes a half sinusoidal form across its width, *B*, and although we initially consider the case where the BM is positioned arbitrarily across the cochlear partition, most of the simulations are performed assuming that the BM is positioned at the side, as both shown in Fig. A1.

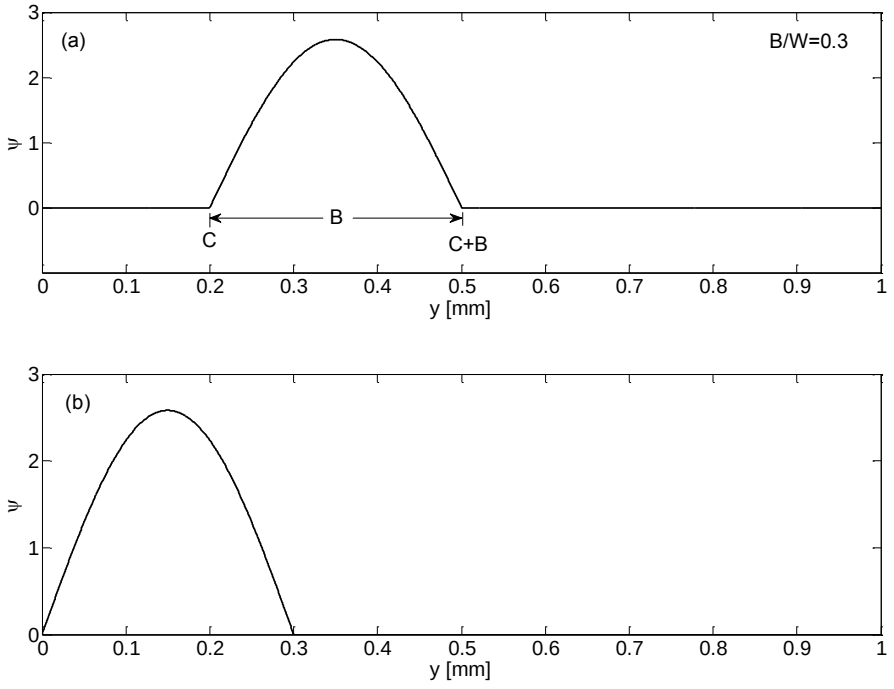

Fig. A 1 *General form of the velocity distribution across the partition (a) and specific case used in the simulations here (b).*

Thus for the general case, in our coordinate system,

$$\psi(y) = \sqrt{\frac{2W}{B}} \sin\left(\frac{\pi(y-C)}{B}\right), \tag{A21}$$

for y = C to $B + C$ and $\psi(y) = 0$ for $y = 0$ *to* C and $B+C$ to W.

where the factor of $\sqrt{\frac{2W}{B}}$ ensures that $\psi(y)$ is normalised in the way defined in equation (A7).

In this case it can be shown that the coupling coefficient defined in equations (A14) and (A15) is equal to

$$A_0 = \frac{2}{\pi}\sqrt{\frac{2B}{W}} \tag{A22}$$

for $n = 0$ and for $n \geq 1$ is equal to

$$A_n = \frac{2}{\pi}\sqrt{\frac{2B}{W}}\left(\frac{W^2}{W^2 - n^2B^2}\right)\left[\cos\left(\frac{n\pi C}{W}\right) + \cos\left(\frac{n\pi(C+B)}{W}\right)\right]. \tag{A23}$$

In the special case where the BM is to one side of the cochlear partition, so C is equal to zero, then

$$A_n = \frac{2}{\pi}\sqrt{\frac{2B}{W}}\left(\frac{W^2}{W^2 - n^2B^2}\right)\left[1 + \cos\left(\frac{n\pi B}{W}\right)\right]. \tag{A24}$$

The coupling coefficients in this thus only depend on the mode order, n, and the BM width relative to the overall width of the cochlear, B/W, which is often written as ε, so that

$$A_0 = \frac{2}{\pi}\sqrt{2\varepsilon}, \text{ and for } n \geq 1, \quad A_n = A_0 \frac{1 + \cos(n\pi\varepsilon)}{1 - n^2\varepsilon^2}. \tag{A25, A26}$$

As ε becomes smaller, the amplitude of the higher order modes is more pronounced. Fig. A2 shows the variations of $Q(k)/H$ with kH for various values of ε. The choice of the values of ε used to illustrate these curves is driven by the desire to ensure that $n^2\varepsilon^2$ is never zero in the range of summation used, which otherwise causes numerical

problems in equation (A26). A total of 30 terms have been used in the series approximation of $Q(k)$ in equation (A20) to produce the graphs shown in Fig. A2, but the results are almost indistinguishable if twice this number of terms is used, suggesting that the series has converged.

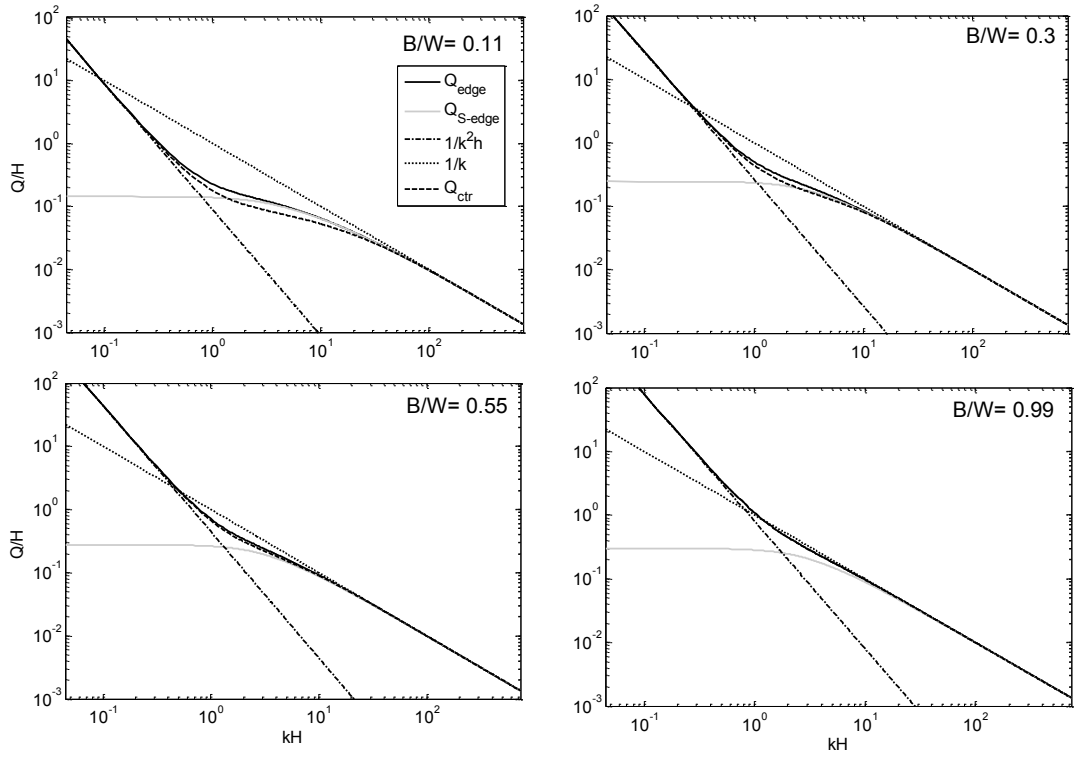

Fig. A 2 *The normalised fluid coupling impedance Q(k)/H as a function of normalised wavenumber, kH, for B/W equal to 0.11 (a), 0.3 (b), 0.55 (c) and 0.99 (d). The results are plotted for the BM both at the edge and at the centre (dashed) of the cochlear partition, together with the low wavenumber limit of Q(k) equal to $1/k^2h$ (dot-dashed) and the high wavenumber limit (dotted) of Q(k) equal to 1/k. The short wavelength component, derived by subtracting the long wavelength component, $1/k^2h$, from the total impedance is also shown as a faint solid line.*

The pressure associated with the first term in equation (A20) corresponds to the $n = 0$ mode shape in equation (A9) and has no radial variation. It thus corresponds to that of the two-dimensional model described by de Boer (1991), for example. Using equation (A22), this term can be written in the present case as

$$Q_{2\mathrm{D}}(k) = \frac{8B}{\pi^2 W k}\coth(kH). \qquad \text{(A27)}$$

Further using the long wavelength approximation, that the wavelength is large compared to *H*, so that *kH* is significantly less than unity, equation (A26) reduces to that for the one-dimensional fluid model,

$$Q_{1D}(k) = \frac{8B}{\pi^2 W H k^2}. \tag{A28}$$

The differential equation for the one-dimensional fluid coupling model in the symmetric cochlea can be written as

$$\frac{\partial^2 p(x)}{\partial x^2} = -\frac{2i\omega\rho}{h} v(x), \tag{A29}$$

where *h* can be considered as the "effective" height of the cochlear channel.

Equation (A29) is most often derived by assuming that the pressure difference, $p(x)$, and longitudinal fluid velocity, $u(x)$, are uniform across the cochlear cross section, and that the longitudinal fluid velocity is related to the transverse BM velocity by the conservation of mass equation, which for an incompressible fluid can then be written as

$$\frac{\partial u(x)}{\partial x} = \frac{v(x)}{h}. \tag{A30}$$

Combining this with the equation for conservation of momentum in this case,

$$\frac{\partial p(x)}{\partial x} = -2i\omega\rho\, u(x), \tag{A31}$$

by differentiating equation (A30) with respect to *x* and substituting into equation (A31), yields equation (A29).

Assuming that $p(x)$ and $v(x)$ are again expressed as $P(k)e^{-ikx}$ and $V(k)e^{-ikx}$ and that the ratio of $P(k)$ to $V(k)$, $Z_{FC}(k)$ is written as $i2\omega\rho Q(k)$, then $Q_{1D}(k)$ in this case is equal to

$$Q_{1D}(k) = \frac{1}{hk^2}. \tag{A32}$$

Comparing equations (A32) and (A28), the effective height can be expressed as

$$h = \frac{\pi^2 WH}{8B}, \tag{A33}$$

where WH is the area of each channel. The assumed BM motion in equation (A21) corresponds to that of a beam with hinged boundary conditions. Steele and Taber (1979) also consider clamped beam boundary conditions, for which the transverse BM mode shape is proportional to $\sin^2(\pi y/B)$, in which case the equivalent value of h, in our notation, is $3WH/2B$. The effective height, h, is thus again proportional to WH/B but with the constant of proportionality being 1.5, instead of about 1.23 in equation (A33). This illustrates how the results are relatively insensitive to the exact mode shape of the transverse BM velocity, which is, in fact more closely modelled as having a hinged boundary condition at one end and a clamped boundary condition at the other (Homer *et al.* 2004).

Instead of using a single term in the expansion of the coth(kH) term in $Q_{2D}(k)$ to get $Q_{1D}(k)$, we could use the two-term approximation (Neely, 1985) to give the approximation

$$Q_{2D} = \frac{1}{k^2 h} + T_{2D}, \tag{A34}$$

where

$$T_{2D} = \frac{8BH}{3\pi^2 W}, \tag{A35}$$

which is the thickness of an added mass which acts only locally. This can be interpreted in the same way as the end correction that is used to represent the near field effect of a number of higher-order terms in the acoustics of an organ pipe, and, like the end correction, T is proportional to the characteristic length of the vibrating system, which is the BM width, B, in this case. The constant of proportionality is equal to $8/3\pi^2$, if we assume that W is equal to H, i.e., about 0.27. In fact if all the terms in equation (A20) are taken into account in this series, we can express the

thickness of the added mass, using equation (A23) when the edge of the BM is a distance C from one side of the cochlear partition, as

$$T = \frac{8BH}{3\pi^2 W} + \sum_{n=1}^{\infty} \frac{4B}{n\pi^3} \coth\left(\frac{n\pi H}{W}\right)\left[\frac{\cos(n\pi C/W) + \cos(n\pi(C+B)/W)}{1 - n^2 B^2/W^2}\right]^2, \qquad \text{(A36)}$$

so that T is about $0.22W$ or $0.8B$ when $B = W/3$ and the BM is on the edge of the cochlear partition. This thickness also corresponds to the limiting value of $Q_S(k)$ in equation (2.8) as k tends to zero, so that, as seen in Fig. 2.1,

$$\lim_{k \to 0} Q_S(k) = T. \qquad \text{(A37)}$$

The value of the effective thickness, normalised by both W and B, is plotted in Fig. A3, as a function of the normalised BM width, B/W, for the BM at the edge and at the centre of the cochlear partition dividing the fluid chambers. These results were calculated using equation (A36), although the numerical results obtained from individual evaluation of equation (A37) using curves such as those in Fig. A2 are in excellent agreement. Although only about 30 terms are again required for convergence of the series in equation (A36) when B/W is above about 0.1, as required for convergence of equation (A20) to get Fig. A2 above, rather more terms are required for convergence when B/W is smaller than 0.1. This is because of the very large number of higher order modes that are excited when the source becomes small compared with the size of the duct.

When B/W is equal to unity the BM extends over the whole width of the fluid chamber so that the problem becomes almost two-dimensional and both T/W and T/B tend to about 0.27, as calculated above. When B/W becomes much less than unity, however, and the BM is in the centre of the cochlear partition, both sides of the BM element are essentially radiating into a three-dimensional space. The effective thickness is then equal to about twice the end correction for a piston in a baffle, which is about $1.7B$ (Kinsler *et al.*, 1982), assuming an equivalent radius of B, which is similar to the value observed in Fig. A3. Also, when B is much smaller than W but the BM is on the edge of the cochlear partition, the effect of the side wall will be to double the pressure in front of the vibrating BM element and hence to approximately double the value of T/B, as also observed in Fig. A3.

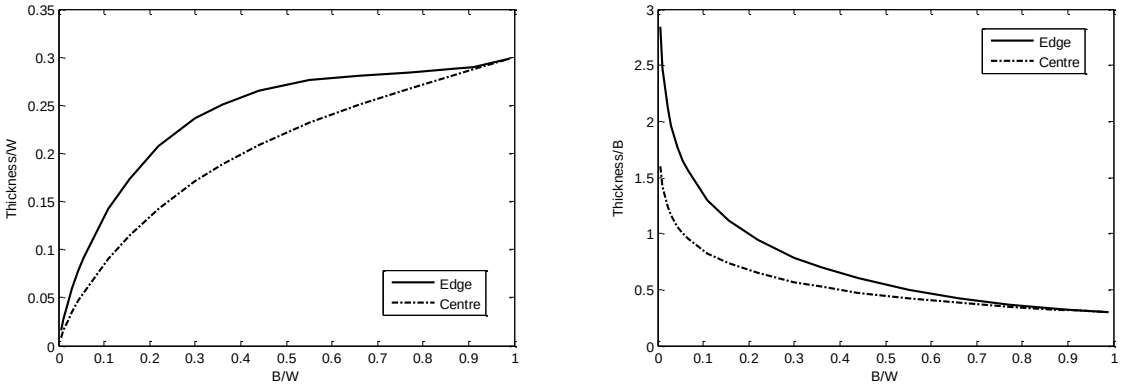

Fig. A 3 *Variation of the effective thickness of the fluid loading, normalised by the width of the fluid chamber, T/W(left), and when normalised by the BM width, T/B (right) as a function of the normalised BM width, B/W, for the BM both at the edge (solid) and the centre (dashed) of the cochlear partition.*

The corresponding variation of the short wavelength pressure in the cochlear with *B*/*W* is shown in Fig. A4. This extends the range of short wavelength contributions that can be calculated over the results shown in Fig. 2.5, which was calculated for *B*/*W* equal to 0.3, so that it can be used in Section 4 to calculate the full fluid coupling at different positions along a non-uniform cochlea. In fact, apart from the amplitude variation, the shape of these short wavelength components is relatively independent of *B*/*W*. As noted in Section 2, however, their magnitude is determined by the fact that the integral of the continuous pressure or the sum of the discrete pressures must add up to that given using the thickness of the equivalent mass in equation (A36).

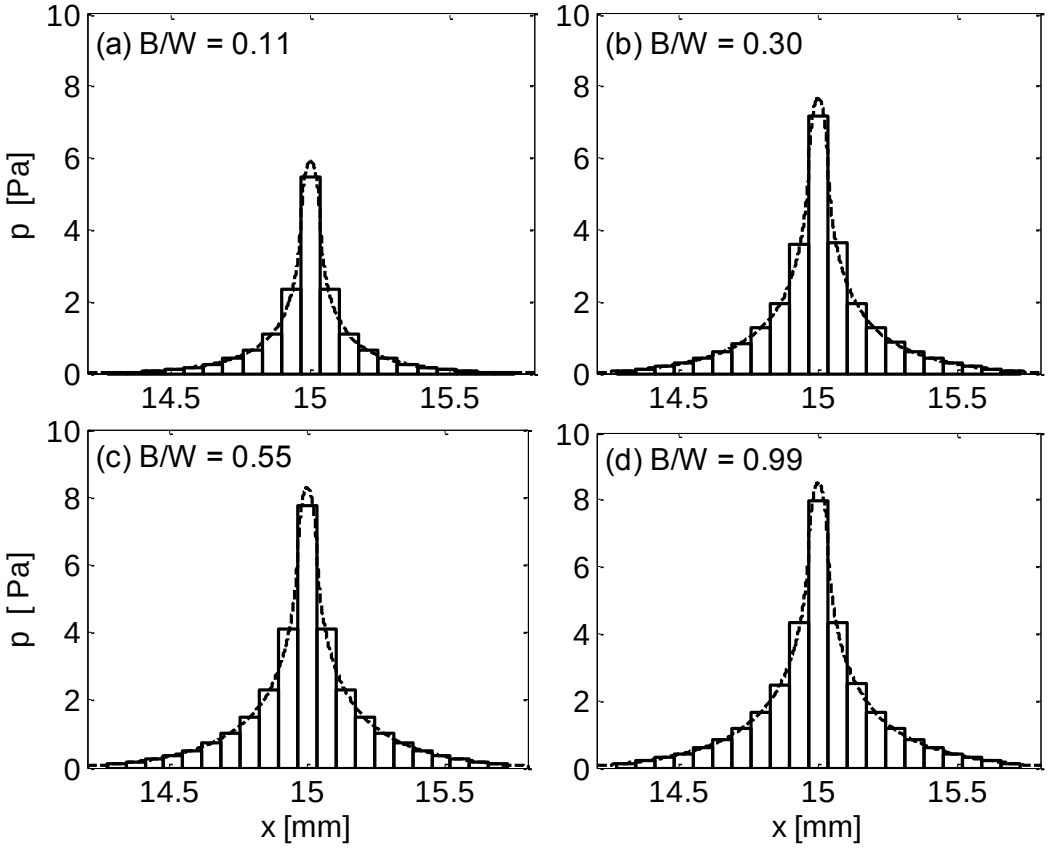

Fig. A 4 *The variation of the modal pressure due to the short wavelength component of fluid coupling along the cochlea for B/W = 0.11, 0.3, 0.55, 0.99(dashed curve) together with the average pressure over the discrete elements (solid lines).*

An alternative method of calculating the short wavelength component of the model pressure is to move away from the assumption that the longitudinal distribution of the BM velocity is sinusoidal, as in the wavenumber analysis above, by assuming that only one element of the BM is moving. The analysis of acoustic modes in a duct, developed by Morse and Ingard (1968) and Doak (1973), can then be used to calculate the near field pressure distribution and hence the modal pressure due to this discrete source distribution.

Following Doak (1973), we first express the complex pressure due to a point monopole source of volume velocity q_0 at location $x = 0$, $y = y'$, $z = z'$ within a single cochlear chamber, modelled as a hard walled duct, as

$$p_c(x,y,z) = \sum_{m=0}^{\infty} B_m \phi_m(y,z) e^{-ik_m x}, \tag{A38}$$

where only a forward travelling wave is assumed, m denotes a duo of modal integers, m_1 and m_2, k_m is the modal wavenumber and $\phi_m(y, z)$ represents the assumed acoustic mode shapes, which are orthonormal so that

$$\int_{y=0}^{W}\int_{z=0}^{H}\phi_n(y,z)\phi_m(y,z)dydz = WH, \tag{A39}$$

only if n is equal to m and is otherwise zero. The modal amplitude is given by

$$B_m = \frac{\omega\rho q_0}{2Ak_m}\phi_m(y',z'), \tag{A40}$$

where A is the cross-sectional area of the chamber, which is WH in this case. For a rectangular chamber with rigid walls the mode shapes can be written as

$$\phi_m(y,z) = \sqrt{\varepsilon_{m_1}\varepsilon_{m_2}}\cos\left(\frac{m_1\pi y}{W}\right)\cos\left(\frac{m_2\pi z}{H}\right), \tag{A41}$$

where ε_{m_1} and ε_{m_2} are normalisation constants equal to 1 if m_1 or m_2 equal zero and are otherwise equal to 2.

The difference between this formulation and that in equation (A8), apart from the fact that the driving source is now assumed to be a monopole rather than the longitudinally sinusoidal distribution given by equation (A5), is that instead of the wavenumber being a specified value in the analysis above, it is now a variable that changes with the modal order, and the sum of a number of contributions with different wavenumbers goes to make up the pressure in equation (A38).

In the incompressible case assumed here, the modal wavenumber becomes

$$k_m = \pm i\sqrt{\left(\frac{m_1\pi}{W}\right)^2 + \left(\frac{m_2\pi}{H}\right)^2}, \tag{A42}$$

which can be written as $\pm i/l_m$. Provided m_1 and m_2 are not both zero, corresponding to a fast wave of infinite speed, the modal contributions are thus all evanescent, with a longitudinal dependence that can be written as

$$e^{-ik_m x} = e^{-x/l_m}, \tag{A43}$$

where l_m is a modal decay length, assuming that the appropriate root of k_m is chosen so that the pressure decays moving away from the source.

The pressure in the chamber due to the velocity distribution of a whole element of the BM in the discrete model can now also be calculated from equation (A38) by generalising equation (A40) to give the modal amplitude for a distribution of monopole sources (Doak, 1973), which in this case is given by the elemental BM velocity distribution, so that the mode amplitude becomes

$$B_m = \frac{\omega \rho v_0}{2Ak_m} \int_{y=0}^{W} \psi(y)\phi_m(y,0)dy \int_{x=-\Delta}^{0} e^{-x/l_m} dx, \tag{A44}$$

where the first integral is proportional to the parameter A_n defined above.

The modal pressure difference, in equation (A16), due to the near field, or short wavenumber, components, can then be calculated by integrating this pressure over the BM width, to give

$$p_\mathrm{S}(x) = \frac{2}{W} \sum_{m=1}^{\infty} B_m \int_{y=0}^{W} \psi(y)\phi_m(y,0)dy e^{-x/l_m}, \tag{A45}$$

where the integral is again proportional to A_n above. The modal pressure due to the near field of this vibrating element of the BM can thus be written as

$$p_\mathrm{S}(x) = \sum_{m=1}^{\infty} a_m e^{-x/l_m}, \tag{A46}$$

where a_m is the overall modal amplitude, and has a different meaning from the definition in equation (6.14). Each mode has its own decay length l_m, and it is clear from equation (A42) and the definition of l_m that these get increasingly small as m becomes larger, resulting in a more local response, which is enhanced by the fall off in the mode amplitude, a_m, with m. The lowest order evanescent mode, for which m_1 = 0 and m_2 = 1, has a decay length l_m, which is equal to H/π.

Expressing the integrals in equations (A44) and (A45) in terms of A_{m1} and further integrating $p_S(x)$ over the width of an element, the averaged near field pressure at the discrete location n' is

$$p_S(n') = v_0 \sum_{m=1}^{\infty} Z_m e^{-n'\Delta/l_m}, \tag{A47}$$

where

$$Z_m = \frac{i\omega\rho l_m^3 \varepsilon_{m1}\varepsilon_{m2}}{4H\Delta} A_{m1}^2 \left(1 - e^{\Delta/l_m}\right)^2, \tag{A48}$$

where $n' = |n - n_0|$ for an excitation of the n_0-th element.

A reasonable approximation to the averaged pressure across the BM elements, which is the result needed to incorporate this near field component of the pressure into the discrete model, is given by taking only two terms in this modal summation and setting x equal to $n'\Delta$ where Δ is the elemental length so that

$$p_{SA}(n') = \left(Z_1 e^{-n'\Delta/l_1} + Z_2 e^{-n'\Delta/l_2}\right) v_0, \tag{A49}$$

To fit the results shown in Fig. 2.5 for B/W equal to 0.3, Z_1 and Z_2 are equal to 201 Pa·s·m^{-1} and 522 Pa·s·m^{-1}, l_1 is equal to $H/3.47$ and l_2 to $H/12.8$. The pressure amplitudes are selected so that the sum of all the elements, which is equal to

$$\sum_{-\infty}^{\infty} p_{SA}(n') = \left(Z_1 \frac{1 + e^{-\Delta/l_1}}{1 - e^{-\Delta/l_2}} + Z_2 \frac{1 + e^{-\Delta/l_2}}{1 - e^{-\Delta/l_2}} \right) v_0, \tag{A50}$$

is equal to $i2\omega\rho T v_0$, where T is the equivalent thickness of the fluid loading, as defined above, and v_0 is the velocity of the element.

This analysis also suggests an alternative form for the short wavelength value of $Q(k)$, in the wavenumber domain, obtained by taking the Fourier transform of each exponential term in equation (A46). By noting that $p_S(x)$ must be an even function of x, and so $Q_S(k)$ must be entirely real, this can be written as

$$Q_S(k) = \sum_{m=1}^{\infty} \frac{b_m}{\sqrt{1+k^2 l_m^2}}, \tag{A51}$$

where the sum of all the values of b_m must equal T. A reasonable approximation to this series can be obtained by only taking a single term in this series, to that

$$Q_{SA}(k) = \frac{T}{\sqrt{1+k^2 T^2}}, \tag{A52}$$

which tends to T as k becomes small and tends to $1/k$ as k becomes large, in agreement with the properties of $Q_S(k)$.

The sum of the long wavelength component in equation (A32) and this approximation to the short wavelength component is thus

$$Q_A(k) = \frac{1}{k^2 h} + \frac{T}{\sqrt{1+k^2 T^2}}. \tag{A53}$$

The accuracy of this approximation to $Q(k)$ is discussed below, but it is not as good a fit to equation (A20) for values of kH about unity as the polynomial approximation used by de Boer and van Bienema (1982), for example, which can be written as

$$Q^{(3)}(k) = \frac{1+b_0 k^2 h}{k^2 h + d_0 k^3 h}, \tag{A54}$$

where b_0 and d_0 are fitted parameters. Equation (A53) does, however, have the advantage of limiting to $1/k^2 h + T$ for small k, of having no fitted parameters, and of being valid for both positive and negative values of k.

The accuracy of equation (A52) for describing short wavelength fluid coupling is illustrated in Fig. A5, which shows the computed value of $Q_S(k)/Q_{SA}(k)$ as a function of k for various values of B/W. This ratio is unity for very low and very high values of k, as expected since equation (A52) tends to the correct values in these limits. The maximum error is quite large for small values of B/W, the near field of which would require many modal components to approximate, but is only about 12% for B/W equal to 0.3, although the maximum error unfortunately occurs in the wavenumber region

corresponding to the wavelength of the cochlear wave in the active case, $kH \approx 10$ in this case.

This approximation is also illustrated in Fig. A6, which shows the normalised values of $Q(k)$ computed using the full series expression, equation (A20) and the approximation $Q_A(k)$ given by equation (A53) as a function of normalised wavenumber for various values of B/W. The approximation is again better for B/W = 0.30 compared with 0.11, and looks quite reasonable on this rather large logarithmic scale.

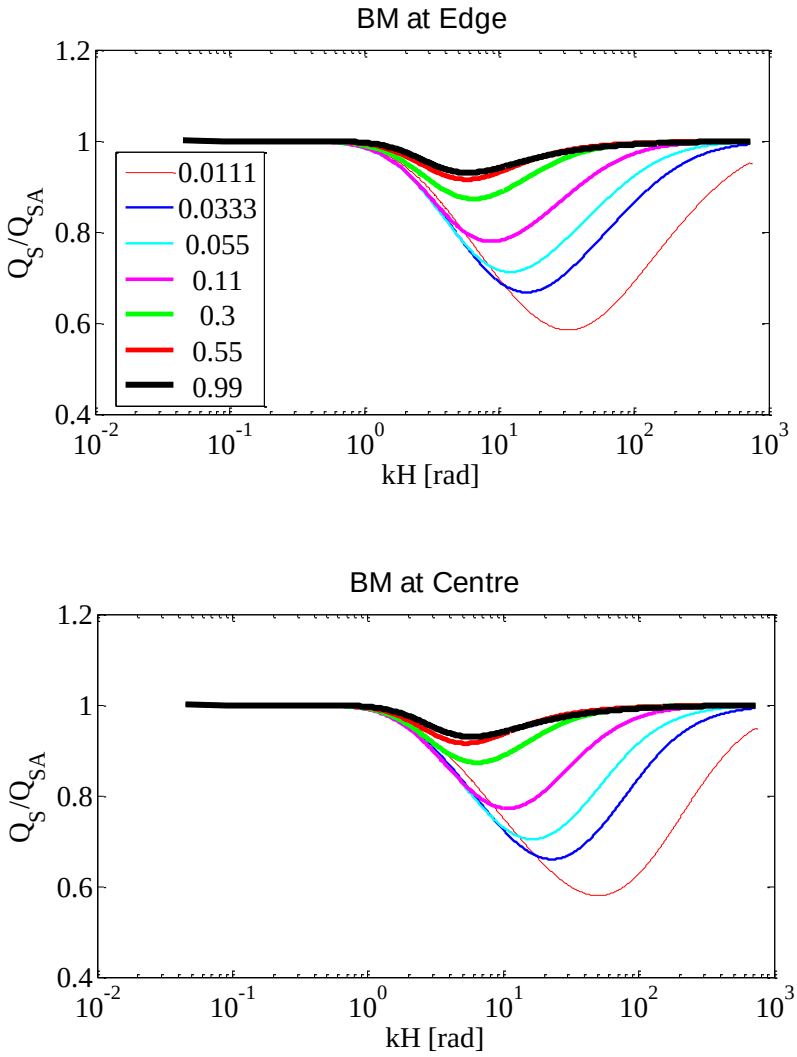

Fig. A 5 *Ratio of the true short wavenumber component of the normalised fluid coupling impedance, $Q_S(k)$ and the approximation given by $Q_{SA}(k)$ equal to* equation (A52) *as a function of normalised wavenumber for various normalised BM widths, B/W, with the BM on the edge of the cochlear partition (above) and at the centre (below).*

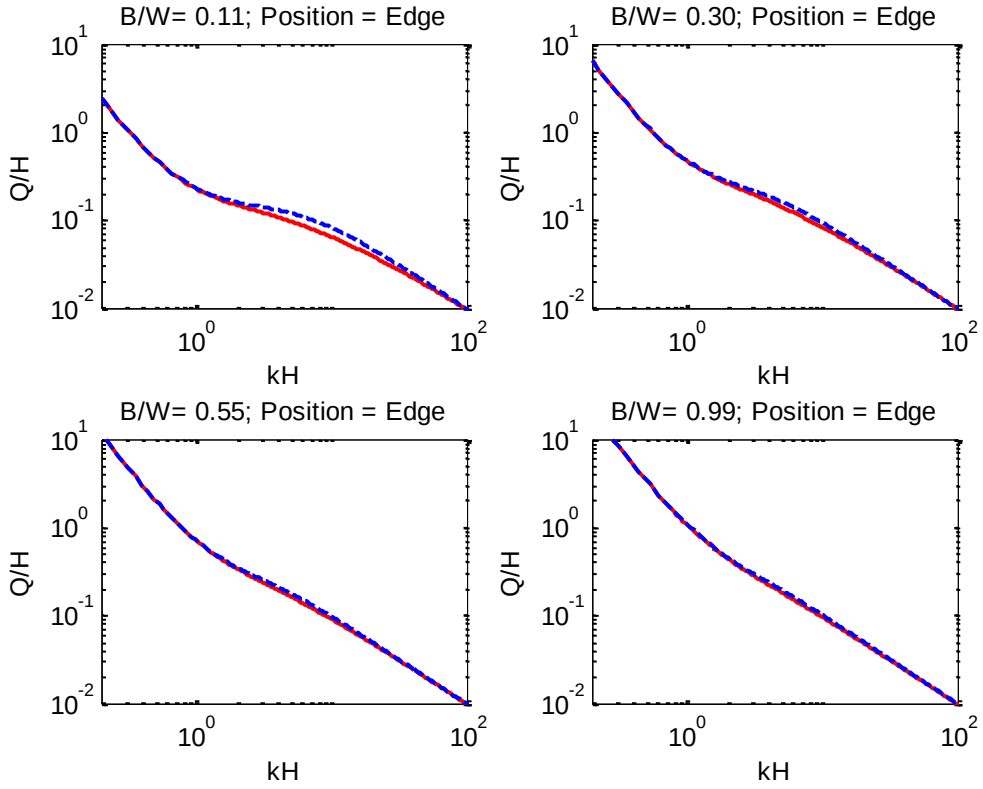

Fig. A 6 *The normalised fluid coupling impedance, $Q(k)/H$ as a function of normalised wavenumber, kH, for B/W equal to 0.11(a), 0.30 (b), 0.55 (c) and 0.99 (d), calculated using the full series formula, equation (A20), and the approximation given by equation (A53).*

References

A.J. Aranyosi, R. Ghaffari and D.M. Freeman (2008) Tectorial membrane travelling waves: A new mechanism for longitudinal coupling. Concepts and Challenges in the Biophysics of Hearing, Keele, World Scientific.

E. de Boer (1982) Correspondence principle in cochlear mechanics. *Journal of the Acoustical Society of America* **71**(6), 1496-1501.

E. de Boer and E. van Bienema (1982) Solving cochlear mechanics problems with higher-order differential equations. *Journal of the Acoustical Society of America* **72**(5), 1427-1434.

E. de Boer (1984) Auditory physics. Physical principles in hearing theory. II. *Physics Reports* **105**(3), 141-226.

E. de Boer (1991) Auditory physics. Physical principles in hearing theory. III. *Physics Reports* **203**, 125-231.

E. de Boer (1996) Mechanics of the Cochlea: Modeling Effects. Chapter 5 in: *The Cochlea* (ed. P. Dallos, A.N. Popper and R.F. Fay). Springer: 258-317.

E. De Boer and M.A. Viergever (1982) Validity of the Liouville-Green (or WKB) method for cochlear mechanics. *Hearing Research* **8**, 131-155.

Cochlear Ltd. (2008) *Technical Specification on Hybrid™ L24 implant.*

O. de La Rochefoucauld, W.F. Decraemer, S.M. Khanna and E.S. Olson (2008) Simultaneous measurements of ossicular velocity and intracochlear pressure leading to the cochlear inut impedance in gerbil. *Journal of the Association for Research in Otolaryngology* **9**, 161-177.

P.E. Doak (1973) Excitation, transmission and radiation of sound from source distributions in hard-walled ducts of finite length (I): The effects of duct cross-section geometry and source distribution space-time pattern. *Journal of Sound and Vibration* **31**(1), 1-72.

S.J. Elliott, E.M. Ku and B. Lineton (2007) A state space model for cochlear mechanics. *Journal of the Acoustical Society of America* **122**(5), 2759-2771.

F.J. Fahy and P. Gardonio (2007) *Sound and Structural Vibration: Radiation, transmission and response,* 2nd ed. Elsevier Academic Press.

C. Fernandez (1952) Dimensions of the cochlea (guinea pig). *Journal of the Acoustical Society of America* **24**, 519-523.

H. Fletcher (1953) *Speech and hearing in communication.* Van Nostrand, reprinted in ASA Edition 1995.

N.H. Fletcher and T.D.Rossing (1998) *The Physics of Musical Instruments*, Springer, 2nd Edition.

D.D. Greenwood (1990) A cochlear position-frequency function for several species – 29 years later. *Journal of the Acoustical Society of America* **87**, 2592-2605.

M. Homer, A. Champneys, G. Hunt and N. Cooper (2004) Mathematical modelling of the radial profile of basilar membrane vibrations in the inner ear. *Journal of the Acoustical Society of America* **116**(2), 1025-1034.

L.E. Kinsler, A.R. Frey, A.B. Coppens, J.V. Sanders (Eds.) (1982) *Fundamentals of Acoustics*, 3rd edition. John Wiley & Sons.

P.J. Kolston (2000) The importance of phase data and model dimensionality to cochlear mechanics. *Hearing Research* **145**, 25-36.

E.L. Le Page (2003) The mammalian cochlear map is optimally warped. *Journal of the Acoustical Society of America* **114**(2), 896-906.

J. Lighthill (1981) Energy flow in the cochlea. *J. Fluid Mechanics* **106**, 149-213.

F. Mammano and R. Nobili (1993) Biophysics of the cochlea: linear approximation. *Journal of the Acoustical Society of America* **93**(6), 3320-3332.

J. Meaud and K. Grosh (2010) The effect of tectorial membrane and basilar membrane longitudinal coupling on cochlear mechanics. *Journal of the Acoustical Society of America* **127**(3), 1411-1421.

A. Moleti, N. Paternoster, D. Bertaccini, R. Sisto and F. Sanjust (2009) Otoacoustic emissions in time-domain solutions of nonlinear non-local cochlear models. *Journal of the Acoustical Society of America* **126**(5), 2425-2436.

P.M. Morse and K.U. Ingard (1968) *Theoretical Acoustics*, McGraw Hill.

P.M. Morse (1948) *Vibration and Sound*. McGraw Hill, 2nd Edition (reprinted in 1981 by the Acoustical Society of America).

S.T. Neely (1981) Finite difference solution of a two-dimensional mathematical model of the cochlea. *Journal of the Acoustical Society of America* **69**(5), 1386-1393.

S.T. Neely (1985) Mathematical modelling of cochlear mechanics. *Journal of the Acoustical Society of America* **78**(1), 345-352.

S.T. Neely and D.O. Kim (1986) A model for active elements in cochlear biomechanics. *Journal of the Acoustical Society of America* **79**(5), 1472-1480.

P.A. Nelson and S.J. Elliott (1992) *Active Control of Sound*. Academic Press.

A. Parthasarathi, K. Grosh and A.L. Nuttall (2000) Three-dimensional numerical modelling for global cochlear dynamics. *Journal of the Acoustical Society of America* **107**(1), 474-485.

L.C. Peterson and B.P. Bogert (1950) A dynamical theory of the cochlea. *Journal of the Acoustical Society of America* **22**(3), 369-381.

L.R. Rabiner and B. Gold (1975) *Theory and Applications of Digital Signal Processing.* Prentice Hall.

M.R. Schroeder (1973) An integrable model for the basilar membrane. *Journal of the Acoustical Society of America* **53**(2), 429-434

C.A. Shera, A. Tubis and C.L. Talmadge (2004) Do forward- and backward-traveling waves occur within the cochlea? Countering the critique of Nobili *et al.* *Journal of the Association for Research in Otolaryngology* **5**, 349-359.

C.A. Shera, A. Tubis and C.L. Talmadge (2005) Coherent reflection in a two-dimensional cochlea: short-wave versus long-wave scattering in the generation of reflection-source otoacoustic emissions. *Journal of the Acoustical Society of America* **118**(1), 287-313.

C.R. Steele and L.A. Taber (1979) Comparison of WKB calculations and experimental results for three-dimensional cochlear models. *Journal of the Acoustical Society of America* **65**(4), 1007-1018.

C.R. Steele, G. Baker, J. Tolomeo and D. Zetes (1993) Electro-mechanical models of the outer hair cell. In *Biophysics of Hair-Cell Sensory Systems* (eds. H. Duifhuis, J.W. Horst, P. van Dijk, S.M. van Netten). Singapore: World Scientific, 207-214.

M. Thorne, A. Salt, J.E. de Mott, M.M. Henson, O.W. Henson, S.L. Gewalt (1999). Cochlear fluid spaces for six species derived from reconstructions of three-dimensional magnetic resonant images. *Journ. American Laryngological, Rhinological and Otological Soc.* **109**(10), 161-168.

L. Watts (2000) The mode-coupling Liouville-Green approximation for a two-dimensional cochlear model. *Journal of the Acoustical Society of America*, **108**(5), Pt. 1, 2266-2271.

J. Zakis and M. Witte (2001) Modelling of the cochlea using Java 3D. *IEEE Engineering in Medicine and Biology Society*, Melbourne, Australia.

G. Zweig, R. Lipes and J.R. Pierce (1976) The cochlear compromise. *Journal of the Acoustical Society of America* **59**(4), 975-982.

J.J. Zwislocki (1953) Review of recent mathematical theories of cochlear dynamics. *Journal of the Acoustical Society of America*, **25**(4), 743-751.

J.J. Zwislocki and E.J. Kletsky (1979) Tectorial membrane: A possible effect on frequency analysis in the cochlea. *Science* **204**, 639-641.

J.J. Zwislocki (2002) Auditory sound transmission. An autobiographical perspective. Lawrence Erlbann Associates, Mahwah, New Jersey.